






Enhanced lift and thrust via the translational motion between the thorax-abdomen node and the center of mass of a butterfly with a constructive abdominal oscillation

Sheng-Kai Chang , Yu-Hsiang Lai , You-Jun Lin , and Jing-Tang Yang ^{*}
Department of Mechanical Engineering, National Taiwan University, Taipei City, Taiwan

 (Received 10 April 2020; revised 11 August 2020; accepted 28 October 2020; published 3 December 2020)

Butterflies fly with an abdomen oscillating relative to the thorax; the abdominal oscillation causes body parts to undulate translationally relative to the center of mass of a butterfly, which could generate a significant effect on flight. Based on experimental measurements, we created a numerical model to investigate this effect in a free-flying butterfly (*Idea leuconoe*). We fixed the motions of wing-flapping and thorax-pitching, and parametrized the abdominal oscillation by varied oscillating phase. To concentrate the analysis on translational dynamics, we used a motion of a thorax-abdomen node, a joint that the thorax and the abdomen rotate about, to express the translational motion of body parts relative to the center of mass. The results show that the abdominal oscillation enhances lift and thrust via the translational motion of the thorax-abdomen node relative to the center of mass. With the abdominal oscillating phase recorded from real butterflies, the abdominal oscillation causes the thorax-abdomen node to move downward relative to the center of mass in downstroke and move upward relative to the center of mass in upstroke. This constructive movement amplifies the wing-flapping speed relative to the center of mass, which enhances the angle of attack and the strength of leading- and trailing-edge vortices on the wings. The wings thereby generate increased values of instantaneous lift and thrust by 50.32% and 32.57% compared to the case of no abdominal oscillation. Natural butterflies are stated to utilize a particular phase offset of abdominal oscillation to fly. With comparing varied oscillating phases, only the abdominal oscillating phase recorded from natural butterflies produces the best constructive effect on the translational motion of thorax-abdomen node, which maximizes the lift and thrust generated on the wings. It clarifies that butterflies use this specific range of abdominal oscillating phase to regulate the translational motion between the thorax-abdomen node and the center of mass to enhance flight. Our work reveals the translational mechanism of the abdominal oscillation, which is as important as the thorax-pitching effect. The findings in this work provide insight into the flight of butterflies and the design of micro aerial vehicles.

DOI: [10.1103/PhysRevE.102.062407](https://doi.org/10.1103/PhysRevE.102.062407)

I. INTRODUCTION

Flying insects, the most ancient and successful flyers on the earth, have characteristically agile and highly maneuverable flight. Unlike traditional artificial aircraft, insects developed a sophisticated flying technique involving flapping their wings. They can immediately take off, hover in air, or change rapidly the flight direction during danger. The flight skill and the morphology of insects motivate human beings to create micro aerial vehicles (MAVs). A MAV is defined as a flying machine of size less than 15 cm and flight speed up to 15 m s^{-1} , and can assist human beings to execute special tasks such as surveillance, rescue, or flying over a complicated terrain [1]. In recent years, scholars have become increasingly dedicated to the study of the flight of insects, expecting that the inspiration from flying insects that evolved from harsh natural selection can be applied to the design of MAVs.

Among insects of multiple kinds, butterflies fly in an extraordinary manner. Morphologically, a butterfly has four wings, two wings on each side. Since on each side the fore and hind wings generally overlap partially with each other during

flight, they are conventionally treated as a single, broad wing with a small aspect ratio ($AR = 1.5\text{-}2.5$) [2,3]. The wing with a small AR enhances the attachment stability of the leading-edge vortex, which is considered to benefit production of lift in insect flight [4–7]. The differential pressure on the wings of a butterfly has been measured up to 10 Pa and is about six to ten times the value of its wing load [8,9]; this potential of a large aerodynamic force suggests the great maneuverability. In addition, compared with other insects, the flapping frequency of butterflies is small; the flapping frequency is about 25 Hz for hawkmoths [10], 33 Hz for dragonflies [11,12], and 10 Hz for butterflies [9,13]. From the view of applied engineering, the small flapping frequency has an advantage of avoiding material damage and can extend the longevity of use.

The unique structure and small flapping frequency of a butterfly accompany a special flight control method. Differently from other insects, butterflies utilize a coupled wing-body motion to fly. As the flapping frequency of butterflies is comparably small compared with other insects, during flapping, the body has sufficient time to respond to the wing motion, causing the motion of wing and body to become highly coupled [9,14]. According to the coupled form, the coupled wing-body motion of a butterfly involves three move-

^{*}Corresponding author: jtyang@ntu.edu.tw

ments: (i) thorax-pitching motion (ii) wing-flapping motion and (iii) abdominal oscillation. For the thorax-pitching motion and the wing-flapping motion, the pitching motion of the thorax alters the flapping direction of wings and affects the orientation of the aerodynamic force generated by the wings. Fei and Yang [15] indicated that a butterfly utilizes the thorax-pitching motion to control flight. Huang and Sun [16] stated that the thorax-pitching motion of butterflies plays a role equivalent to wing rotation of other insects. Lin *et al.* [17] pointed out that the pitching moment of inertia of a butterfly varies significantly due to the wing-flapping motion, which plays a critical factor in flight control. Senda and co-workers [18,19] showed that the wing wake and wing flexibility enhance the thorax-pitching stability of butterflies. Regarding the abdominal oscillation, a butterfly flies with oscillating the abdomen relative to the thorax. The oscillating frequency of the abdomen is nearly the same as those of wing-flapping and thorax-pitching motion [9,14,20], and the abdominal oscillation is considered to constitute another controlling factor of the pitching control in flight of butterflies [21]. Sunada *et al.* [21] and Wilson and Albertani [22] indicated that the abdominal oscillation generates a considerable inertial torque to balance the aerodynamic torque generated by the wings. Yokoyama *et al.* [23] adjusted the mass of abdomen in a simulation and showed that the abdominal oscillation enhances the stability of the thorax-pitching motion. Suzuki *et al.* [24] proposed a numerical scheme of abdominal oscillation to control the thorax-pitching motion by varying the position of the center of mass of the body. Jayakumar *et al.* [25] proposed a numerical control scheme that was combined with abdominal oscillation and a wing lead-lag motion, and controlled the thorax-pitching motion and the flight.

Although abundant research exists on the pitching mechanism and the flight control method in flight of butterflies, the complete control method is not thoroughly clarified. The coupled wing-body motion consists of a rotational and a translational movement. The movements of the wings and abdomen not only causes the thorax to pitch, but also causes the body parts to undulate translationally relative to the center of mass of the butterfly itself. Suzuki *et al.* [26,27] studied the wing mass and indicated that the lift and thrust forces decrease as the wing mass increases, as, for a large wing mass, the body undulates vertically relative to the center of mass and makes the wing relatively lose a part of flapping speed. Kang and co-workers [14,28] indicated that the amplitude of undulation of the thorax increases with the wing-flapping amplitude, but decreases with the wing loading. Sridhar *et al.* [29] indicated that, with the consideration of the coupled wing-body motion of a butterfly, the power consumption for flight decreases. More recently, Sridhar *et al.* [30] proposed a general expression of a coupled wing-body dynamics and counted the effect of the translational motion between the body parts and the center of mass; they indicated that the abdominal oscillation increases the rate of climbing and the forward velocity of a butterfly.

As a butterfly utilizes a transient flight velocity to regulate the generated timing of aerodynamic force [31], the translational motion between the body parts and the center of mass might play an important controlling factor on flight. However, compared to the pitching mechanism, the translational mechanism of a coupled wing-body motion was less

discussed, especially for abdominal oscillation. Regarding the abdominal oscillation, previous authors have shown that the abdominal oscillation generates an inertial torque which alters the pitching motion of a butterfly. As the abdomen accounts for more than half the mass of a butterfly [2,13], it is also expected that the abdominal oscillation generates an inertial force to affect the translational motion between the body parts and the center of mass. According to our knowledge, the only study related to this effect was made by Sridhar *et al.* [30]. In their recent report, they indicated that the rate of climbing and the forward velocity, which imply lift and thrust, are increased with the abdominal oscillation. From our view, we considered that it might be because the abdominal oscillation causes the thorax and wing root to undulate relative to the center of mass of a butterfly in a proper mode, which relatively increases the flapping speed and the aerodynamic force of the wing. The detailed mechanism of the enhanced aerodynamic force was not addressed, and the effect of abdominal oscillation on the translational motion between the body parts and the center of mass needs to be further clarified. To understand the entire flight control mechanism of a butterfly, it is essential to investigate the effect of abdominal oscillation on the translational motion between the body parts and the center of mass, and its influence on flight.

The objective of this work is to clarify the effect of abdominal oscillation on the translational motion between the body parts and the center of mass of a butterfly, and the resulting aerodynamic influence in flight of butterflies. We measured the distribution of mass, the geometry, and the flight kinematics of free-flying butterflies (*Idea leuconoe*), and established a numerical model to simulate the flight for investigation. To focus on the translational effect caused by abdominal oscillation, in the model we fixed the motions of wing-flapping and thorax-pitching, and parametrized the abdomen oscillation by varied oscillating phase. As a thorax-abdomen node is a joint that the thorax (to which the wings attach) and the abdomen rotate about, we used the motion of the thorax-abdomen node to express the translational level of the coupled wing-body motion relative to the center of mass. In addition, to quantify the effect of abdominal oscillation on the aerodynamic force generated on the wings, we analyzed the velocity of airflow acting on the wings based on the second moment of area, which enables the flow structure and the aerodynamic force to be discussed. This paper is organized as follows: In Sec. II, we describe the experimental method, numerical model, and the quantification of the airflow velocity. In Sec. III A, we verify the numerical model. In Secs. III B–III E, we analyze the effect of abdominal oscillation on the translational motion between the thorax-abdomen node and the center of mass, and present a mechanism to explain this effect on flight. The conclusion is made in Sec. IV.

II. MATERIALS AND METHODS

A. Research object and butterfly model

The research butterfly object is *Idea leuconoe*. The number of butterfly samples was 5 ($N = 5$); they were subscribed from Mu Sheng Insect Museum in Nantou, Taiwan.

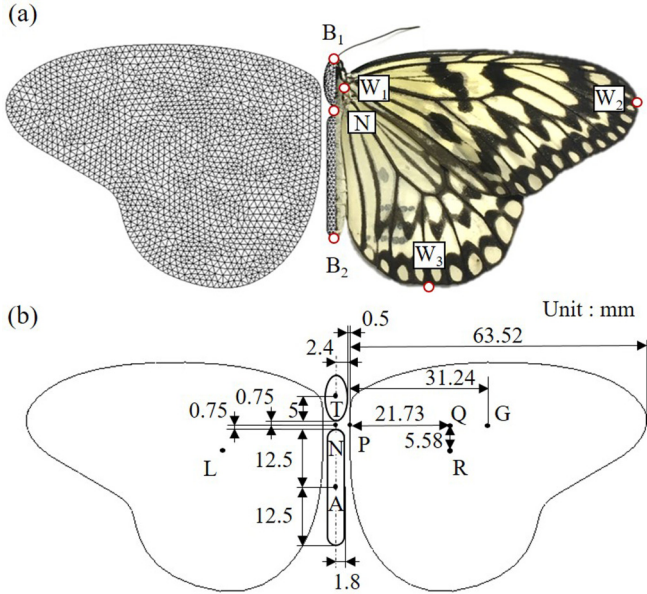


FIG. 1. (a) Comparison in a top view between an experimental butterfly, *Idea leuconoe*, and the butterfly model. (b) Dimensions of the butterfly model. In (a), the butterfly model (right-hand side) is depicted with simulation grids. To illustrate the shape of the grids, the grid size (length of triangular grid) was set to 1.2 mm instead of 0.4 mm that was applied in the simulation.

To establish the numerical flight simulation, we measured mass, geometry, and flight kinematics of butterflies in experiments, and then created a three-dimensional model of a butterfly with software (SOLIDWORKS 2014). Figure 1 and Table I and Table II show a comparison of mass and geometry between the experimental butterflies and the butterfly model. The experimental mass represents wet mass; it was measured on freezing the butterflies at -7°C for 48 h and then dissecting them into several parts. According to the morphology of real butterflies, the butterfly model was assumed to be bilaterally symmetric and consisted of four rigid parts: head-thorax, abdomen, right wing, and left wing. The head-thorax is a prolate ellipsoid (short axis 2.4 mm and long axis 5 mm). The abdomen is an assembly of two hemispheres (radius 1.8 mm) and a cylinder (radius 1.8 mm, length 25 mm). As the wings of real butterflies consist of veins that make them highly anisotropic and difficult to analyze the center of mass during a deformation, the shape of the wings in the model (thickness 0.4 mm) was considered to be nondeformed and was depicted via the photographs of experimental butterflies. To avoid four parts of a butterfly model colliding with

TABLE II. Comparison of dimensions of experimental butterfly and the butterfly model.

		Experiment	Numerical model
Head-thorax	length/mm	10.40 ± 1.29	10.00
	width/mm	4.86 ± 0.71	4.80
Abdomen	length/mm	24.16 ± 2.40	25.00
	width/mm	3.75 ± 0.58	3.60
Wing (single)	span/mm	59.14 ± 4.73	63.52
	mean chord/mm	33.89 ± 3.06	34.73
	aspect ratio	1.75 ± 0.08	1.83

each other, in the model they were separated intentionally by distances 0.5 and 0.75 mm, respectively. As measurement of the actual distribution of density in real butterflies is difficult, the density of each part in the butterfly model was assumed to be individually uniform; under the uniform-density assumption, the position of the center of mass in each part (notation T, A, R, and L in Fig. 1) was calculated directly with the geometry and the mass of the model.

B. Measurement of the flight kinematics in real butterflies

The flying motion in the simulation was based on the realistic motion measured from real butterflies. To measure the real flight kinematics, we used two synchronized high-speed cameras (Phantom v7.3 and Phantom v310) that were aligned orthogonally to photograph the flight of experimental butterflies in a chamber ($35 \times 35 \times 100 \text{ cm}^3$), and used the photographed images to calculate the angles between the body parts [Fig. 2(a)]. The two cameras were both operated at $1000 \text{ frames s}^{-1}$ with pixel resolution 1024×1024 . Before the experiment, we put a cuboid with 1 cm \times 1 cm grids inside the middle of the chamber for calibration; the two cameras were aligned with an optical table to ensure orthogonality. In the experiment, we photographed a single butterfly freely flying in the chamber. The resulting films numbered about 60 in total. We chose ten of them, in which the butterflies flew forward with no turning, to refine the analyzed flying mode. Of ten films in total, each two films corresponded to a single experimental butterfly.

For the calculation of the angles between the body parts, we used software (ImageJ) to mark the coordinates of six feature points on a butterfly in photographed images. These six feature points are a point of wing root, wing tip, wing trailing edge, top of the head, bottom of the abdomen, and the node between the thorax and the abdomen [notation W_1, W_2, W_3, B_1, B_2 , and N in Fig. 1(a)]. Each camera recorded two

TABLE I. Comparison of mass of experimental butterfly and the butterfly model.

	Experiment		Numerical model	
	Mass (g)	Mass ratio (%)	Mass (g)	Mass ratio (%)
Head-thorax	0.138 ± 0.026	30.243 ± 3.962	0.135	30.000
Abdomen	0.249 ± 0.062	55.541 ± 6.066	0.252	56.000
Wings	0.061 ± 0.011	14.216 ± 2.212	0.063	14.000
Total	0.448 ± 0.097	100	0.450	100

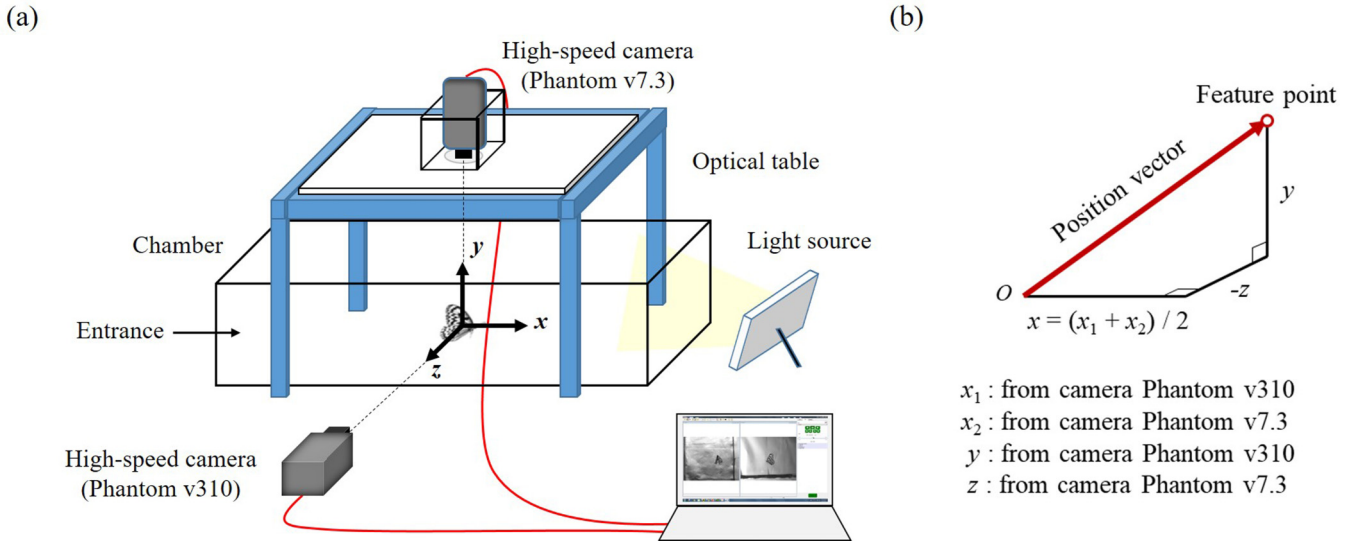


FIG. 2. (a) Experiment schematic diagram. (b) Coordinate measurement.

coordinates of the feature points; with two cameras, the complete three coordinates of each feature point were measured. The y coordinate was measured from the images recorded by Phantom v310. The z coordinate was measured from the images recorded by Phantom v7.3. The x coordinate had two image sources (one from Phantom v310 and the other from Phantom v7.3); the x coordinate was measured by averaging the data recorded from the images of both cameras [Fig. 2(b)]. After measuring the coordinates of the feature points, we used vectors between these feature points to calculate the angle

between the body parts [Fig. 3(a)]. The head-thorax pitching angle (θ) was calculated with vector B_1N and horizontal vector x ; the abdominal oscillation angle (ψ) was calculated with vector B_1N and vector B_2N . The wing-flapping angle (ϕ) was calculated with wing normal vector W_N and body-dorsal vector y_b . The fore-wing sweeping angle (η) was calculated with vector W_2W_1 and wing right-side vector, in which the wing right-side vector is orthogonal to vector B_1N and lies on the wing plane (W_3W_1 - W_2W_1 plane). The flapping period was measured on counting the number of photographs. This

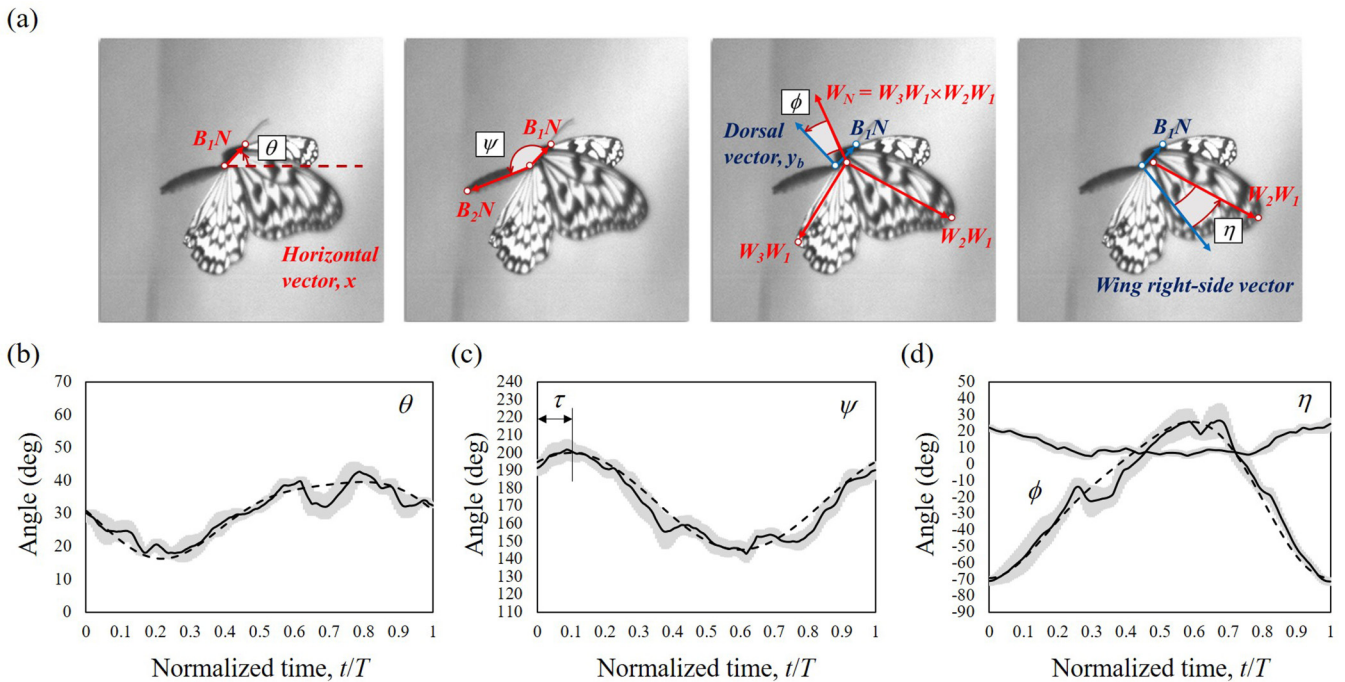


FIG. 3. (a) Calculation of angles and the experimental data of (b) head-thorax pitching angle, (c) abdominal oscillation angle, and (d) wing-flapping and fore-wing sweeping angle. In (b)–(d), the solid black line indicates the average; the grey line indicates the standard error of the mean (SEM); the dashed lines are the approximated motional functions used in the simulation; the normalized time t/T is defined as the actual time divided by a flapping period.

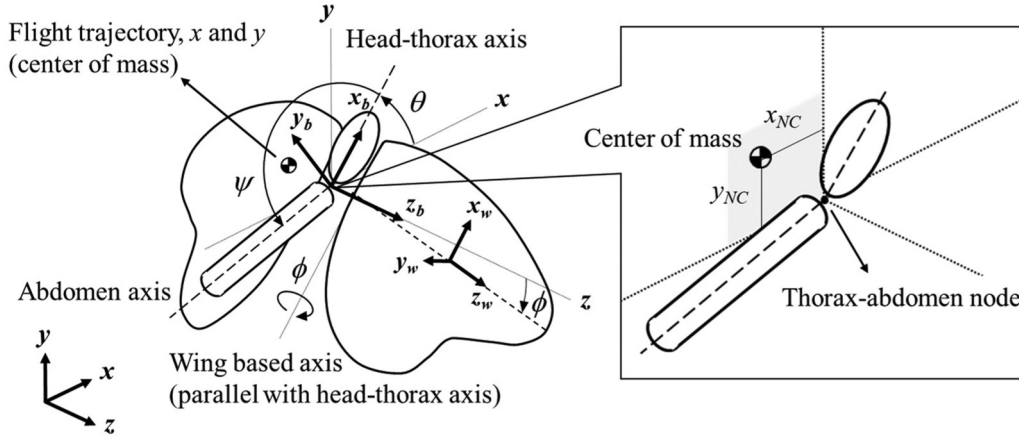


FIG. 4. Definitions of coordinates and motional variables in the butterfly model.

measurement and calculation method has been validated and applied to various animals and insects in our previous research [11,15,31–34].

Figures 3(b)–3(d) show the results of the flight-kinematics experiment. The average flapping period T was 0.117 ± 0.080 s (mean \pm standard deviation). As the fore and hind wings of a butterfly partially overlap each other during flight, structurally restricting the fore-wing sweeping motion [3], in the butterfly model we assumed that the wings do not perform the fore-wing sweeping motion. The inertial effect of fore-wing sweeping motion is to move the body parts relative to the center of mass of a butterfly along the body axis. When the fore-wing sweeps, it does not affect the relative motion of the body parts in the direction perpendicular to the body axis, and does not alter the conclusion of the present study.

C. Definitions of coordinates and motional variables in the model

Three coordinate systems were adopted to describe the motion of the butterfly model Fig. 4. The global coordinates xyz is an inertial frame referred to the ground with axes respectively representing the front, upper, and right side. The body coordinates $x_b y_b z_b$ are a body-fixed frame attached to the head-thorax part, of which the x_b axis coincides with the long axis of the head-thorax; its origin is at the thorax-abdomen node (N, shown in Fig. 1). The wing coordinates $x_w y_w z_w$ are a body-fixed frame attached to the right wing with its x_w , y_w , and z_w axes representing the chordwise, normal, and spanwise directions of the wing respectively; its origin was at the center of mass of the right wing (R, shown in Fig. 1).

As the butterfly model is bilaterally symmetric, the flight trajectory of the center of mass of the butterfly model is restricted to the $x - y$ plane. There are five degrees of freedom (DOF), described with five scalar variables: x , y , θ , ψ , and ϕ . x and y are the horizontal and vertical displacements of the center of mass of the butterfly respectively. The head-thorax and the abdomen can rotate individually about the thorax-abdomen node in direction z . The head-thorax pitching angle θ is defined as an angle between the head-thorax axis x_b and the horizontal axis x ; the angle of abdominal oscillation ψ is defined as an angle between the abdominal axis and the head-thorax axis. Wings can rotate about the wing-based axis;

this axis is through junction P (shown in Fig. 1) and is parallel with the head-thorax axis x_b . The flapping angle ϕ is defined as an angle between the wing span axis z_w and axis z_b . The movement of the wings is, notably, described with the flapping angle, the head-thorax pitching angle, and the motion of the thorax-abdomen node as the wing-based axis is parallel with the head-thorax axis which pitches about the thorax-abdomen node.

The global coordinates, body coordinates, and wing coordinates are transformed among each other with the following matrix. For a vector \mathbf{a} ,

$$[\mathbf{a}]_{xyz} = \begin{bmatrix} \cos\theta & -\sin\theta & 0 \\ \sin\theta & \cos\theta & 0 \\ 0 & 0 & 1 \end{bmatrix} [\mathbf{a}]_{x_b y_b z_b} \quad (1)$$

and

$$[\mathbf{a}]_{xyz} = \begin{bmatrix} \cos\theta & -\sin\theta\cos\phi & \sin\theta\sin\phi \\ \sin\theta & \cos\theta\cos\phi & -\cos\theta\sin\phi \\ 0 & \sin\phi & \cos\phi \end{bmatrix} [\mathbf{a}]_{x_w y_w z_w}. \quad (2)$$

D. Kinetics equations, inertial force, and the motion of thorax-abdomen node in the model

In simulation, the butterfly model flies by propelling itself by simultaneously pitching its head-thorax, flapping wings and oscillating the abdomen. For the rotational movement, head-thorax pitching angle θ and wing-flapping angle ϕ are prescribed as functions approximated with a discrete Fourier transform (DFT; $n = 2$) from the experimental data [Eqs. (3) and (4); dashed lines in Figs. 3(b) and 3(d)]. To analyze the effect of the abdominal oscillation, the abdomen oscillating angle ψ is given as a single cosine function, and is parametrized by a phase offset with $\tau = 0, 0.1, 0.25, 0.5, 0.75$, and $\psi = 180^\circ$ [Eqs. (5) and (6)]. The real abdominal oscillation recorded from the experimental butterflies corresponds to $\tau = 0.1$ [Fig. 3(c)]. In Eqs. (3)–(5), T is the flapping period and was set as 0.1 s.

For the translational movement, the horizontal and vertical accelerations of the center of mass of the butterfly model, \ddot{x} and \ddot{y} in Eqs. (7) and (8), were calculated with an instantaneous aerodynamic force through a computational fluid-dynamic method (CFD; Sec. II E). According to the conservation of momentum, the motion of the thorax-abdomen node relative to the center of mass depends on the relative movements of a butterfly: head-thorax pitching θ , wing flapping ϕ , abdomen oscillation ψ , and their time derivatives. After determining these rotational variables, the motion of the

thorax-abdomen node relative to the center of mass, \ddot{x}_{NC} and \ddot{y}_{NC} , can be consequently solved through the kinetic equations of multirigid bodies [Eq. (9)]. In Eqs. (7)–(9), F_x and F_y are the lift and thrust, respectively; g is the acceleration of gravity (9.81 m s^{-2}). m is the total mass (0.45 g). m_T , m_A , m_{RW} , and m_{LW} are the masses of head-thorax, abdomen, right wing (0.0315 g), and left wing (0.0315 g), respectively (Table I). r_{TN} , r_{AN} , r_{QP} , and r_{RQ} denote the displacements between the body parts (Fig. 1),

$$\theta(t) = 30.070^\circ - 1.571^\circ \cos\left(\frac{2\pi t}{T}\right) - 13.283^\circ \sin\left(\frac{2\pi t}{T}\right) + 2.457^\circ \cos\left(\frac{4\pi t}{T}\right) - 1.622^\circ \sin\left(\frac{4\pi t}{T}\right), \quad (3)$$

$$\phi(t) = -19.321^\circ - 44.044^\circ \cos\left(\frac{2\pi t}{T}\right) - 10.391^\circ \sin\left(\frac{2\pi t}{T}\right) - 6.103^\circ \cos\left(\frac{4\pi t}{T}\right) + 5.432^\circ \sin\left(\frac{4\pi t}{T}\right), \quad (4)$$

$$\psi(t) = 172.5^\circ + 27.5 \cos\left(\frac{2\pi t}{T} - 2\pi \tau\right); \tau = 0, 0.1, 0.25, 0.5, \text{ and } 0.75, \quad (5)$$

$$\psi(t) = 180^\circ \text{ (no abdominal oscillation)}, \quad (6)$$

$$m\ddot{x} = F_x, \quad (7)$$

$$m\ddot{y} = F_y - mg, \quad (8)$$

$$\begin{aligned} m \begin{bmatrix} \ddot{x}_{NC} \\ \ddot{y}_{NC} \\ 0 \end{bmatrix} = & -\frac{d^2}{dt^2} \left\{ m_T \begin{bmatrix} \cos\theta & -\sin\theta & 0 \\ \sin\theta & \cos\theta & 0 \\ 0 & 0 & 1 \end{bmatrix} \begin{bmatrix} r_{AN} \\ 0 \\ 0 \end{bmatrix} \right\} - \frac{d^2}{dt^2} \left\{ m_A \begin{bmatrix} \cos(\theta + \psi) & -\sin(\theta + \psi) & 0 \\ \sin(\theta + \psi) & \cos(\theta + \psi) & 0 \\ 0 & 0 & 1 \end{bmatrix} \begin{bmatrix} r_{AN} \\ 0 \\ 0 \end{bmatrix} \right\} \\ & - \frac{d^2}{dt^2} \left\{ m_{RW} \begin{bmatrix} \cos\theta & -\sin\theta \cos\phi & \sin\theta \sin\phi \\ \sin\theta & \cos\theta \cos\phi & -\cos\theta \sin\phi \\ 0 & \sin\phi & \cos\phi \end{bmatrix} \begin{bmatrix} -r_{RQ} \\ 0 \\ r_{QP} \end{bmatrix} \right\} \\ & - \frac{d^2}{dt^2} \left\{ m_{LW} \begin{bmatrix} \cos\theta & -\sin\theta \cos\phi & -\sin\theta \sin\phi \\ \sin\theta & \cos\theta \cos\phi & \cos\theta \sin\phi \\ 0 & -\sin\phi & \cos\phi \end{bmatrix} \begin{bmatrix} -r_{RQ} \\ 0 \\ -r_{QP} \end{bmatrix} \right\}. \end{aligned} \quad (9)$$

In Sec. III C, we discuss each inertial force generated by the head-thorax, abdomen and wing acting on the motion of the thorax-abdomen node relative to the center of mass. From Eq. (9), the inertial forces generated by the head-thorax ($F_{\text{inert},T}$), the abdomen ($F_{\text{inert},A}$) and the wings ($F_{\text{inert},W}$) were respectively defined in Eqs. (10a)–(10c),

$$F_{\text{inert},T} \equiv -\frac{d^2}{dt^2} \left\{ m_T \begin{bmatrix} \cos\theta & -\sin\theta & 0 \\ \sin\theta & \cos\theta & 0 \\ 0 & 0 & 1 \end{bmatrix} \begin{bmatrix} r_{AN} \\ 0 \\ 0 \end{bmatrix} \right\}, \quad (10a)$$

$$F_{\text{inert},A} \equiv -\frac{d^2}{dt^2} \left\{ m_A \begin{bmatrix} \cos(\theta + \psi) & -\sin(\theta + \psi) & 0 \\ \sin(\theta + \psi) & \cos(\theta + \psi) & 0 \\ 0 & 0 & 1 \end{bmatrix} \begin{bmatrix} r_{AN} \\ 0 \\ 0 \end{bmatrix} \right\}, \quad (10b)$$

$$\begin{aligned} F_{\text{inert},W} \equiv & -\frac{d^2}{dt^2} \left\{ m_{RW} \begin{bmatrix} \cos\theta & -\sin\theta \cos\phi & \sin\theta \sin\phi \\ \sin\theta & \cos\theta \cos\phi & -\cos\theta \sin\phi \\ 0 & \sin\phi & \cos\phi \end{bmatrix} \begin{bmatrix} -r_{RQ} \\ 0 \\ r_{QP} \end{bmatrix} \right\} \\ & - \frac{d^2}{dt^2} \left\{ m_{LW} \begin{bmatrix} \cos\theta & -\sin\theta \cos\phi & -\sin\theta \sin\phi \\ \sin\theta & \cos\theta \cos\phi & \cos\theta \sin\phi \\ 0 & -\sin\phi & \cos\phi \end{bmatrix} \begin{bmatrix} -r_{RQ} \\ 0 \\ -r_{QP} \end{bmatrix} \right\}, \end{aligned} \quad (10c)$$

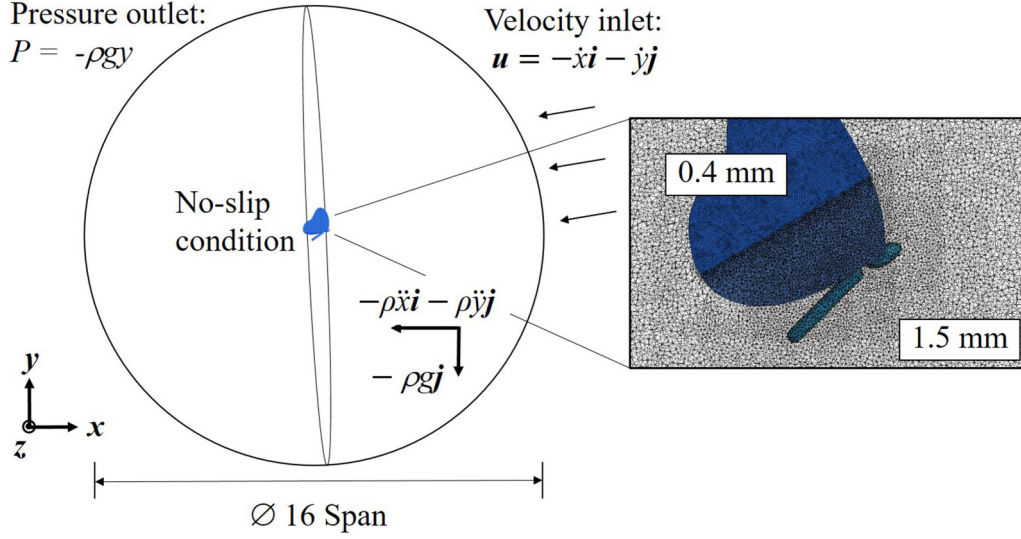


FIG. 5. Boundary conditions and topology of fluid domain grids.

E. Numerical scheme

The flow field was solved numerically with a pressure-based solver (FLUENT) in which we compiled the butterfly model and the kinematic equations of a butterfly [Eqs. (3)–(9)], written in C language. The Reynolds number (Re) of a natural flight of butterfly is 10^3 – 10^4 . We assumed the flow field to be incompressible and laminar, and neglected heat transfer. The medium, air, is a Newtonian fluid of density $\rho = 1.225 \text{ kg m}^{-3}$, viscosity $\mu = 1.7894 \times 10^{-5} \text{ Pa s}$. Because the flight simulation requires a large space for flying, we solved the flow field in a relative frame that moved translationally with the center of mass of the butterfly. In this frame, the butterfly seems fixed at the origin, experiencing an incoming airflow and a virtual acceleration of which the values are exactly opposite the flight velocity and the flight acceleration, respectively. The governing equations of the flow field are

$$\frac{\partial \rho}{\partial t} + \nabla \cdot (\rho \mathbf{u}) = 0, \quad (11)$$

$$\rho \left(\frac{\partial \mathbf{u}}{\partial t} + \mathbf{u} \cdot \nabla \mathbf{u} \right) = -\nabla P + \mu \nabla^2 \mathbf{u} + \rho \mathbf{g} + \rho \mathbf{a}_s, \quad (12)$$

in which \mathbf{u} is a flow velocity field, P is a pressure field, and $\rho \mathbf{a}_s$ is the virtual force per volume due to the coordinate transformation in which $\mathbf{a}_s = -\ddot{x}\mathbf{i} - \ddot{y}\mathbf{j}$. Initially, the butterfly model takes off from rest in still air; the initial conditions of the flow field are $\mathbf{u} = 0$ and $P = -\rho g y$. The flow domain is a sphere of diameter 16 times the wing span. The boundary condition at the inlet is $\mathbf{u} = -\dot{x}\mathbf{i} - \dot{y}\mathbf{j}$, and at the outlet is $P = -\rho g y$. On the surface of the butterfly, there is a no-slip boundary condition.

For the numerical updating, in each time step the flight displacement and velocity were updated through the acceleration that was calculated from Eqs. (7)–(9) with the Euler method. For pressure-velocity coupling, the semi-implicit method for pressure-linked equations consistent (SIMPLEC) was applied. For spatial discretization, the Green-Gauss node-based and

the second-order upwind methods were applied. For the dynamic mesh strategy, a smoothing and a local-remeshing method were adopted. The topology of the fluid domain grid was a tetrahedron; near the butterfly, the grid size was set as 1.5 mm, and on the surface of butterfly, the grid size was set as 0.4 mm (see Fig. 5). The total grid number of the entire fluid domain was 5.2×10^7 . The time interval was set as 0.000 25 s (400 steps per flapping period).

F. Nondimensional variables and definition of angles of attack

The coefficient of thrust (C_T), lift (C_L), horizontal inertial force ($C_{I,x}$), and vertical inertial force ($C_{I,y}$) were normalized with the mean wing-tip velocity and the wing area. In Eq. (13), $2fS\Delta\phi$ is the mean wing-tip velocity during a flapping cycle; $2S\bar{c}$ is the surface area of two wings. S and \bar{c} are the length (63.52 mm) of the wing span and mean chord length (34.73 mm; Table I), respectively. $\Delta\phi$ is the total flapping amplitude [95° ; Fig. 3(d)];

$$C_T, C_L, C_{I,x}, \text{ and } C_{I,y} \equiv \frac{F}{\frac{1}{2}\rho(2fS\Delta\phi)^2(2S\bar{c})}. \quad (13)$$

In Sec. III D, we analyzed the aerodynamic force and the flow structure with the velocity of airflow acting on the wing. As it is difficult to quantify the actual velocity of airflow acting on the wing, with reference to previous works [7,35], we used a point G , which is the point of the second moment of area of the wing, to estimate the velocity of airflow. Point G specifies the radius of the second moment of area (31.24 mm) in the spanwise direction from the wing-basis point P , and is in line with the thorax-abdomen node N (Fig. 1). We assumed that the value of the velocity of airflow striking the wing (\mathbf{V}_a) is opposite to the value of the velocity of the point G relative to the ground [\mathbf{V}_G ; Eq. (14)]. With this assumption, we defined the airflow speed ($\sqrt{V_{a,xw}^2 + V_{a,yw}^2 + V_{a,zw}^2}$), chordwise-plane airflow speed ($\sqrt{V_{a,xw}^2 + V_{a,yw}^2}$), and the angles of attack (α and β) in the wing coordinates [Fig. 6, Eqs. (15) and (16)].

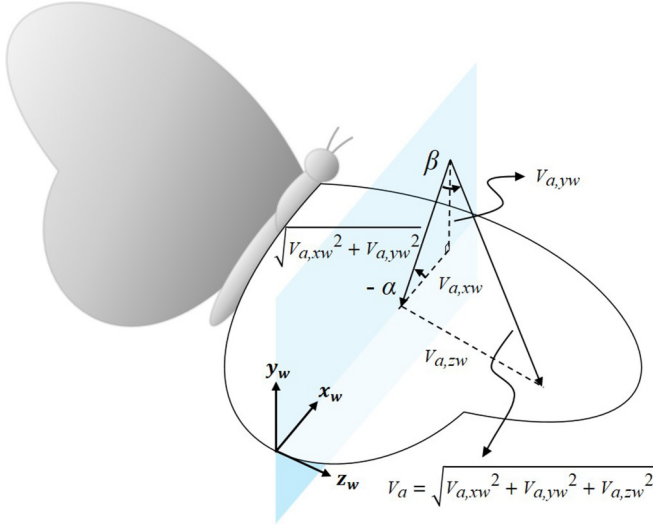


FIG. 6. Airflow speed and angle of attack based on the second moment of area of the wing.

In Eqs. (15) and (16), α represents the angle of attack lying on the chordwise plane; β represents the deviation level from the chordwise plane. A positive value of α indicates that air flows from the ventral surface to the dorsal surface of the wing; a positive value of β indicates that air flows from the wing root to the wing tip;

$$\mathbf{V}_a = -\mathbf{V}_G, \quad (14)$$

$$\alpha = \sin^{-1} \left(\frac{V_{a, xw}}{\sqrt{V_{a, xw}^2 + V_{a, yw}^2}} \right), \quad (15)$$

$$\beta = \sin^{-1} \left(\frac{V_{a, zw}}{\sqrt{V_{a, xw}^2 + V_{a, yw}^2 + V_{a, zw}^2}} \right). \quad (16)$$

III. RESULTS AND DISCUSSION

A. Validation of the model

The main results that we present were obtained through a numerical method; in this section we verify our numerical model by comparing the numerical model with experimental data. Figure 7 is a comparison of the flying motion between the numerical butterfly model and the experiment. The

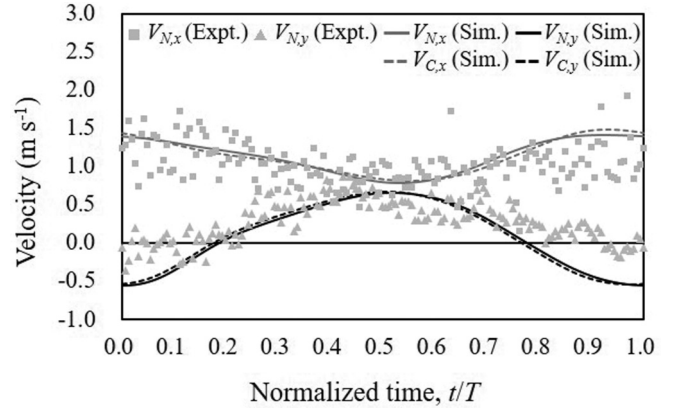


FIG. 8. Comparison of flight velocity between experiment and simulation at the 30th flapping cycle. The triangles and squares depict the average velocity of the thorax-abdomen node (V_N) measured from the experimental butterflies ($N = 5$) in every sampling time, and the solid and dashed lines are respectively the velocities of the thorax-abdomen node (V_N) and the center of mass (V_C) calculated in the simulation.

head-thorax pitching, wing flapping, and abdominal oscillation in the model are given based on the experimental data [Fig. 3; Eqs. (3)–(5) with $\tau = 0.1$]. In Fig. 7, the flying motion of the model is in satisfactory accordance with the experimental photographs.

Figure 8 is the comparison of the flight velocity in the 30th flapping cycle between the numerical simulation and the experimental butterflies. The reason to choose the 30th flapping cycle is that our butterfly model takes off from rest, hence requiring time to attain a periodically stable flying state in which the values of flight velocity and aerodynamic force become periodic. The period required to attain a periodically stable state is about 10–15 cycles (Fig. 13). To ensure accuracy, we chose the 30th flapping cycle for comparison. In Fig. 8, the horizontal flight velocity calculated in the simulation lies in the range of the experimental data. The vertical velocity has overall the same trend, but has a smaller value at the end of the upstroke ($t/T = 0.8-1$). The reason is that, for a real butterfly, a butterfly is reported to use selectively a clap-and-fling mechanism with its flexible wings at the end of the upstroke to generate an additional lift [21,36,37]. As the simulation model adopted the average flying motion with rigid wings [Eqs. (3)–(5); Figs. 3(b)–3(d)], the butterfly in the model did not perform the clap-and-fling mechanism

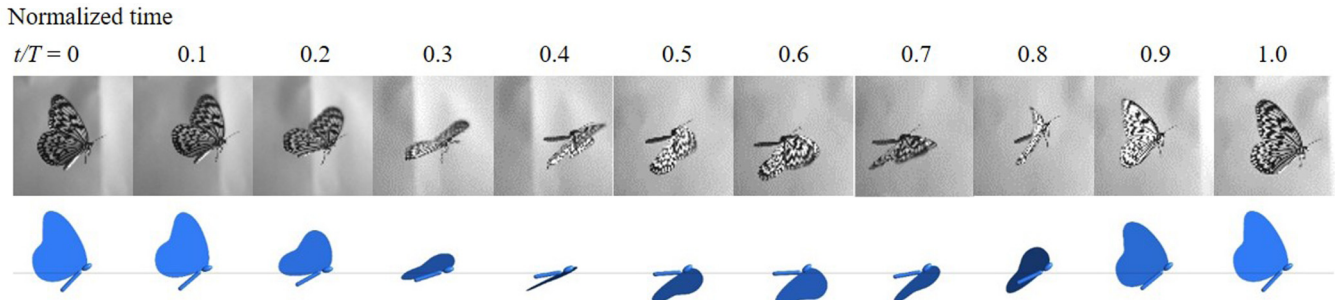


FIG. 7. Comparison of flying motion between an experimental butterfly and the simulation model.

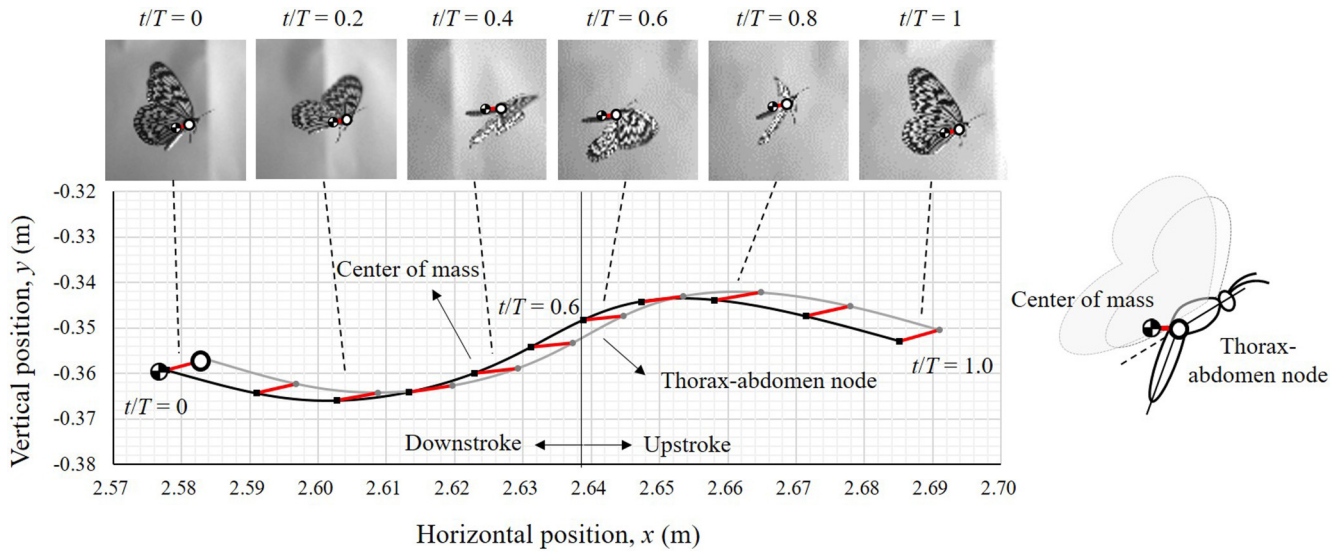


FIG. 9. Flight trajectories of the center of mass and the thorax-abdomen node in the 30th cycle of the simulation. The black and grey curves respectively represent the trajectory of the center of mass of the butterfly and the thorax-abdomen node; the red line represents the displacement between them.

effectively. Nevertheless, the clap-and-fling mechanism appears only at the end of the upstroke, and an insect does not always utilize it to generate lift [36,37]. Some studies had thus ignored the clap-and-fling mechanism. From the flow field discussed in Sec. III D (Figs. 16 and 17), the nature of vortices in the simulation agrees with the experimental observation [38,39]. In addition, the translational mechanism of the abdominal oscillation mainly occurs at about mid-downstroke and mid-upstroke (see details in Sec. III D). The absence of the clap-and-fling mechanism at the end of the upstroke thus does not alter the effect of abdominal oscillation, and does not change the conclusion of the present study. From the comparison between the simulation and the experimental data and the discussion above, the numerical model of the present study shows a sufficient effectiveness and reliability.

B. Translational motion of the thorax-abdomen node relative to the center of mass

Butterflies fly with oscillating an abdomen relative to thorax; the abdominal oscillation causes the thorax-abdomen node to move translationally relative to the center of mass, which may generate a significant effect on flight. In this section, we analyzed the translational motion between the thorax-abdomen node and the center of mass. The translational motion between the thorax-abdomen node and the center of mass shown in Fig. 9 (red line) is, notably, not the thorax-pitching motion that served to describe the pitching mechanism in previous work.

Figure 9 shows the trajectories of the thorax-abdomen node and the center of mass in the 30th cycle of the flight simulation. The motions of head-thorax pitching, wing flapping, and abdominal oscillation in the simulation are given based on the experimental measurement [Fig. 3; Eqs. (3)–(5) with $\tau = 0.1$]. In Fig. 9, the flight trajectory of the center of mass (black line) shows a “jumped” pattern. The reason is that in Fig. 10, during the downstroke ($t/T = 0 - 0.6$), the

downward-flapping wings mainly generate a positive lift and a negative thrust; during the upstroke ($t/T = 0.6 - 1$), the upper-backward flapping wings mainly generate a negative lift and a positive thrust. The center of mass hence begins to climb at the beginning of the downstroke and decreases the climbing velocity in the upstroke. In contrast, Fig. 9 shows that the motion of the thorax-abdomen node relative to the center of mass (red line) has an opposite trend to that of the center of mass. At the beginning of the downstroke ($t/T = 0$), the thorax-abdomen node moves downward relative to the center of mass, and attains its lowest point about the end of the downstroke ($t/T = 0.6$). Then, during the upstroke ($t/T = 0.6 - 1$), it moves upward relative to the center of mass and attains its highest point at the end of the upstroke ($t/T = 1$). In Fig. 11, the vertical velocity of the thorax-abdomen node relative to the center of mass, $V_{NC,y}$, shows a negative value in the downstroke and a positive value in the upstroke.

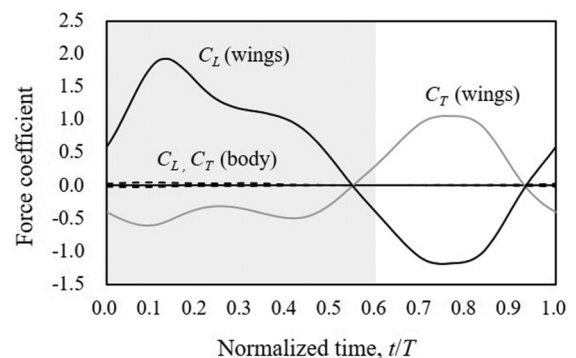


FIG. 10. Lift and thrust coefficients in the 30th cycle of the simulation. The solid black and grey lines are respectively the lift and thrust on the wings; the dashed lines (approximately lying on the horizontal axis) are the lift and thrust on the body which includes head, thorax, and abdomen.

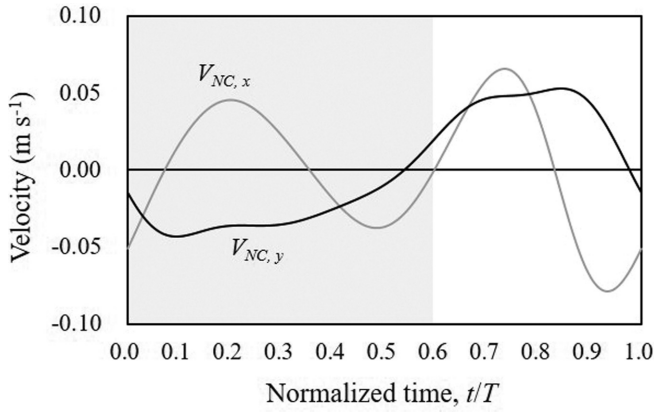


FIG. 11. Velocity of the thorax-abdomen node relative to the center of mass of the butterfly in the 30th cycle of the simulation.

Because the wings are connected to the thorax that rotates about the thorax-abdomen node, the motion of the thorax-abdomen node relative to the center of mass affects the motion of wings. As discussed in the preceding paragraph, the motion of thorax-abdomen node has an opposite trend to that of the center of mass. During the downstroke ($t/T = 0 - 0.6$), when the wings flap downward, the center of mass is accelerated upward. The downward speed of the thorax-abdomen node

relative to the center of mass, instead, leads the wings to resist the upward acceleration of the center of mass, and causes the wings to flap in a faster downward speed relative to the center of mass. For the same reason, during the upstroke ($t/T = 0.6 - 1$), the center of mass is accelerated downward; the upward speed of thorax-abdomen node relative to the center of mass leads the wings to flap in a faster upward speed relative to the center of mass. This phenomenon shows that the motion of thorax-abdomen node relative to the center of mass amplifies the flapping speed of wings. In addition, a butterfly utilizes a pressure-drag-based force to fly [8,40]; this pressure force causes the center of mass to accelerate. Nevertheless, the opposite tendency of the motion of thorax-abdomen node relative to the center of mass (red line in Fig. 9) indicates that the thorax-abdomen node makes the wings flap against the pressure drag in a faster speed, which implies an enhancement of aerodynamic force.

C. Distinct flight performance via the motional interference between the thorax-abdomen node and the wings with varied abdominal oscillation

The translational motion between the thorax-abdomen node and the center of mass in a real butterfly leads the wings to flap against the air drag in an increased speed, providing a potential enhancement of aerodynamic force. To investigate

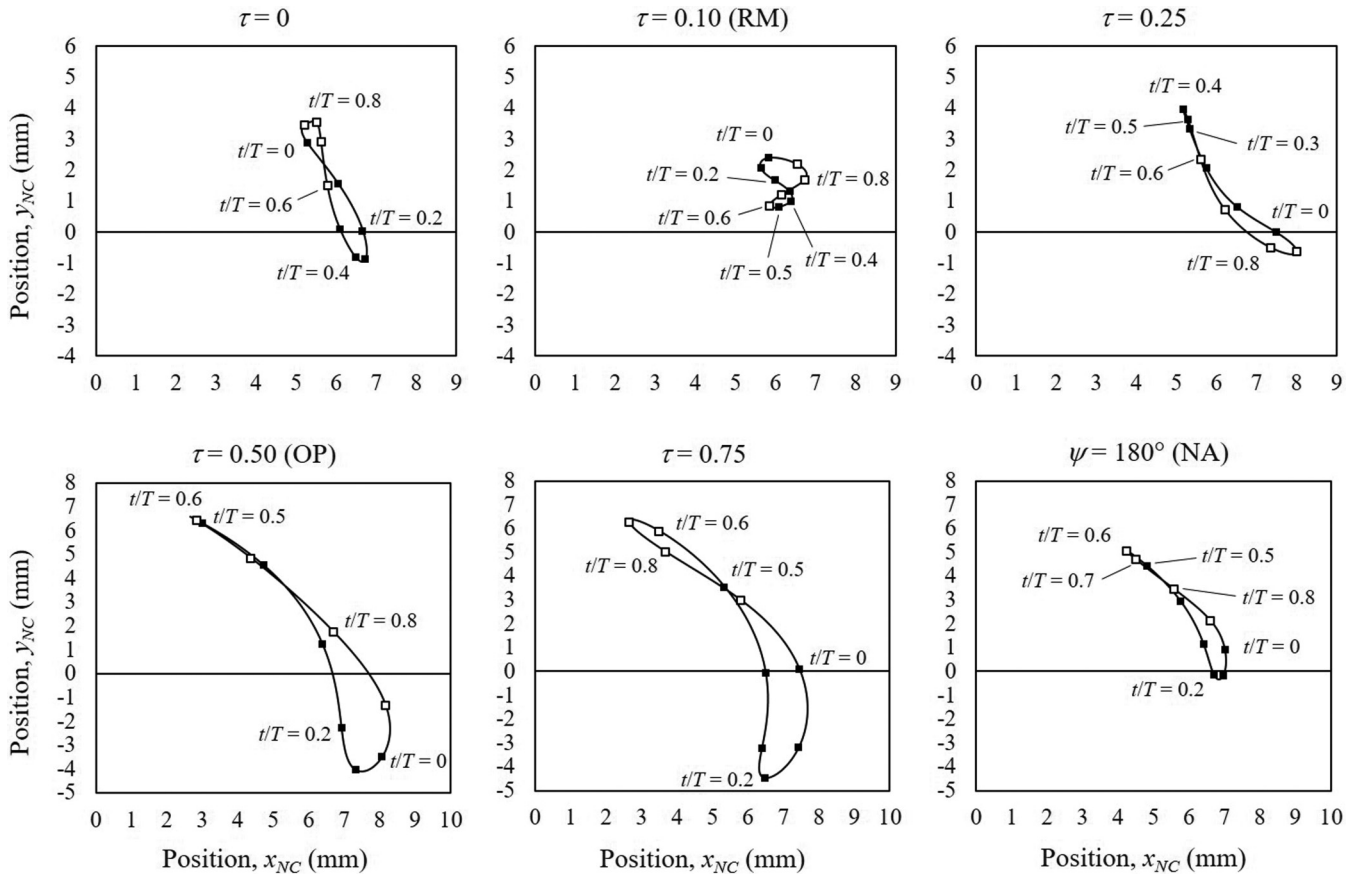


FIG. 12. Trajectories of the thorax-abdomen node relative to the center of mass with varied phase offset of abdominal oscillation. In each case, the black dot represents the trajectory of the thorax-abdomen node during a downstroke ($t/T = 0 - 0.6$); the white dot represents the trajectory of the thorax-abdomen node during an upstroke ($t/T = 0.6 - 1$). The center of mass of the butterfly is located at origin.

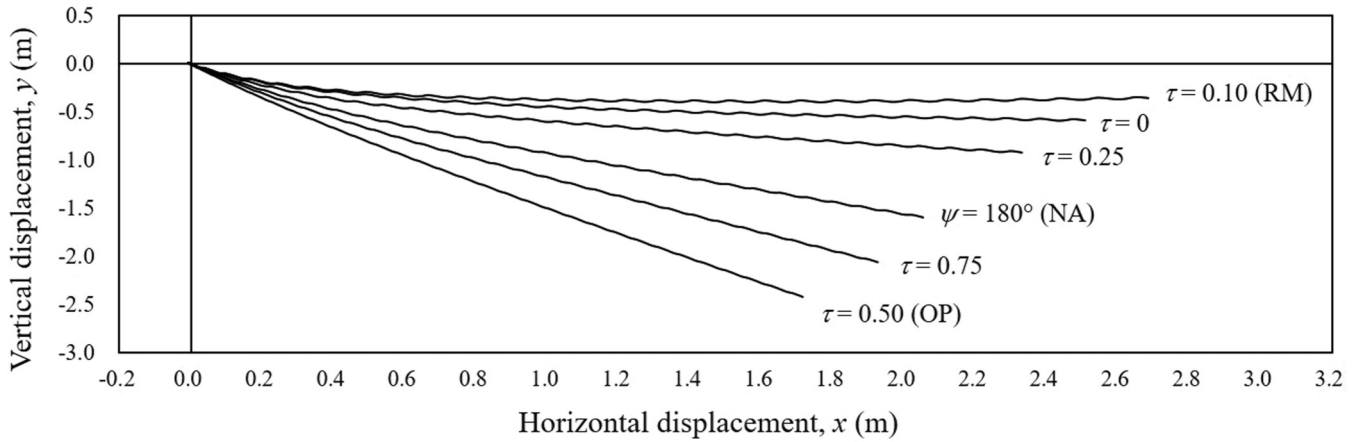


FIG. 13. Flight trajectories (center of mass) with varied phase offset of abdominal oscillation in 30 cycles after take-off.

the effect of abdominal oscillation, we fixed the head-thorax pitching motion and the wing-flapping motion [Eqs. (3) and (4)], and parametrized the abdominal oscillation by an oscillating phase offset [Eqs. (5) and (6)].

Figures 12 and 13 show the trajectories of thorax-abdomen node relative to the center of mass with varied phase of abdominal oscillation and the corresponding flight trajectories. In Fig. 12, the trajectory pattern of the thorax-abdomen node relative to the center of mass significantly varies from case to case, and the resulting flight trajectories are distinct (Fig. 13). The case with the same phase of abdominal oscillation recorded from the real butterflies ($\tau = 0.1$; RM) flies the highest and the most rapidly; the case with the opposite phase of abdominal oscillation ($\tau = 0.5$; OP) flies the lowest and the most slowly. This indicates that through oscillation, the abdomen changes the translational motion of thorax-abdomen node relative to the center of mass, and makes the wings flap in different manners which results in the distinct flight trajectories.

On analysis of the correlation between the motion of thorax-abdomen node and the flight (Figs. 12 and 13), we found that the movement direction of the thorax-abdomen node relative to the center of mass plays a critical factor in controlling the flight. According to the moving direction of the thorax-abdomen node relative to the center of mass, we classified that into two sets: (i) a constructive motion and (ii) a destructive motion. Figure 14 is a schematic diagram of these two sets. In Fig. 14(a), for the case of constructive motion, the movement direction of the thorax-abdomen node relative to the center of mass is the same as that of the wing-flapping; the wings therefore obtain an additional flapping speed relative to the center of mass due to the translational motion between the thorax-abdomen node and the center of mass. In contrast, for the case of destructive motion [Fig. 14(b)], the movement direction of the thorax-abdomen node relative to the center of mass is opposite to that of the wing-flapping; the wings therefore partially lose their flapping speed relative to the center of mass due to the translational motion between the thorax-abdomen node and the center of mass. Figure 12 shows that the cases with $\tau = 0.1$ and $\tau = 0$ are the constructive cases and have superior flight trajectories (Fig. 13). The cases with $\tau = 0.25, 0.5, 0.75$ and $\psi = 180^\circ$ are the destructive cases

(Fig. 12) and have deteriorated flight trajectories (Fig. 13). The cases with $\tau = 0.1$ and $\tau = 0.5$ are the two extreme cases that correspond to the completely constructive and destructive cases respectively (Fig. 12; $\tau = 0.1$ and $\tau = 0.5$), and are also the best and worst for flight (Fig. 13; $\tau = 0.1$ and $\tau = 0.5$). The case with $\psi = 180^\circ$ is a special case. In this case, the abdomen does not oscillate relative to the thorax; the remaining factor to affect the motion of the thorax-abdomen node relative to the center of mass is, therefore, the flapping motion of the mass-possessed wings. In such a situation, the thorax-abdomen node appears as a destructive motion (Fig. 12; $\psi = 180^\circ$). Suzuki and co-workers [26,27], who studied the effect of wing mass, had similar results to ours. Nevertheless, in additionally considering the abdominal oscillation, our results indicate that abdominal oscillation can recover the negative effect of the wing mass by leading the thorax-abdomen node to move relative to the center of mass in the same direction of the wing-flapping, and makes the butterfly fly more highly and rapidly.

To summarize, the abdominal oscillation alters the translational motion of the thorax-abdomen node relative to the center of mass, and produces an interference on the motions of the thorax-abdomen node and the wings. The wings thereby gain or lose a part of flapping speed relative to the center of mass, resulting in the distinct flights. In this work, we individually prescribed the rotational movement of the wings and the head-thorax as a single function [θ and ϕ ; Eqs. (3) and (4)], which means that the wing-flapping and head-thorax pitching motions do not vary in all cases. Therefore, the mechanism we present here, that the abdominal oscillation controls flight through the translational motion between the thorax-abdomen node and the center of mass, is not the rotational mechanism according to which the abdomen produces an inertial torque to alter the thorax-pitching motion of a butterfly.

D. Velocity of incoming airflow, vortex structure, and aerodynamic force

The abdominal oscillation produces a motional interference on the motions of the thorax-abdomen node and the wings, which affects the wing-flapping speed relative to the center of mass and the flights. To quantify this effect, we

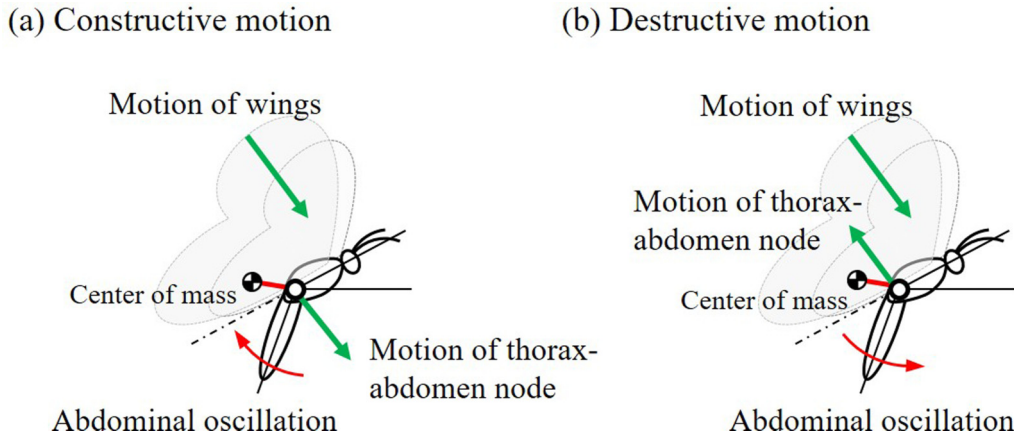


FIG. 14. Schematic diagrams of (a) constructive motion and (b) destructive motion produced by abdominal oscillation.

calculated the velocity of incoming airflow striking the wings. To eliminate a factor due to the various flying modes shown in Fig. 13, in this section the flight velocity (the velocity of the center of mass) in all cases are prescribed as the flight velocity that is calculated from the motion of a real butterfly (Fig. 8; $V_{C,x}$ and $V_{C,y}$). The details of the calculation of flight velocity and incoming airflow are described in Secs. IID and IIF. For the sake of brevity, we present three representative cases with oscillating phases $\tau = 0.1$, $\tau = 0.5$, and $\psi = 180^\circ$, which respectively represent a completely constructive, a completely destructive interference, and the case of no abdominal oscillation (Fig. 12). The profile of other cases is presented in the Appendix.

Figures 15(a) and 15(b) are the comparison of the incoming airflow speed and the angle of attack among these three cases. Overall, the case with $\tau = 0.1$ has the largest incoming airflow speed and angle of attack, and the case with $\tau = 0.5$ has the smallest incoming airflow speed and angle of attack. This trend is consistent with the lift and thrust coefficients shown in Figs. 15(c) and 15(d), which indicates that the method to calculate the speed of incoming airflow and angle of attack presented in Sec. IIF is appropriate to quantify the distinctness and the varied trend of the aerodynamic force in the flight of a butterfly.

For details of the airflow velocity and the resulting aerodynamic force, Fig. 15(a) shows that at the mid-downstroke (t/T

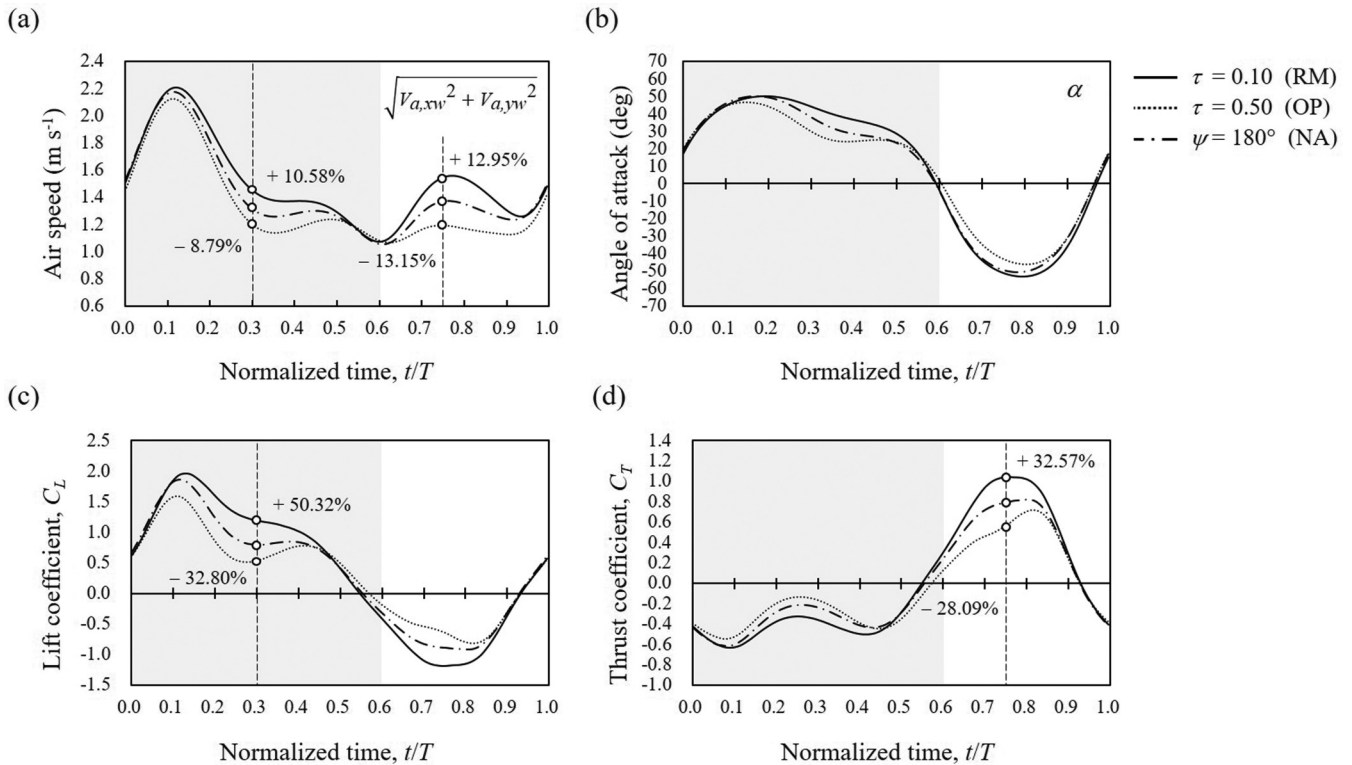


FIG. 15. (a) Speed of incoming airflow, (b) angle of attack, (c) lift coefficient, and (d) thrust coefficient on the wings.

$t/T = 0.3$) and mid-upstroke ($t/T = 0.75$), compared with the case of no abdominal oscillation ($\psi = 180^\circ$), the value of the incoming airflow speed in the case with $\tau = 0.1$ respectively increases 10.58% and 12.95%. In contrast, the value of the incoming airflow speed in the case with $\tau = 0.5$ respectively decreases 8.79% and 13.15%. The instantaneous values of lift and thrust generated on the wings therefore respectively increases 50.32% and 32.57% in the case with $\tau = 0.1$, and decreases 32.8% and 28.09% in the case with $\tau = 0.5$ [Figs. 15(c) and 15(d)]. As the flight velocity (the velocity of the center of mass relative to the ground) is the same in these cases, the distinctness shown in Fig. 15 indicates that, via the translational motion between the thorax-abdomen node and the center of mass, the abdominal oscillation with $\tau = 0.1$ increases the flapping speed of the wings relative to the center of mass, and leads the wings to suffer an increased incoming airflow velocity and generate an increased aerodynamic force.

Figures 16 and 17 are the vortex structure and the pressure contour in the cases with $\tau = 0.1$ and $\tau = 0.5$ during a downstroke and an upstroke, respectively. In Fig. 16, at the beginning of the downstroke ($t/T = 0.1 - 0.3$), a leading-edge vortex (LEV_d ; the subscript d denotes forming in downstroke) and a trailing-edge vortex (TEV_d) form on the dorsal surface of the wing. Near a wing root, the LEV_d attaches to the wing surface, and near a wing tip, it detaches from the wing. The TEV_d , in contrast, detaches from the wing immediately once it forms. At the mid-downstroke ($t/T = 0.3$), a wing-tip vortex (WTV_d) is observed forming at the wing tip. The shape of the WTV_d is like an annulus which encircles the LEV_d . Meanwhile, a part of the WTV_d merges with the LEV_d , constituting a complex $LEV_d - WTV_d$ structure and afterwards detaching from the wing. During the later stage of the downstroke ($t/T = 0.3 - 0.6$), the LEV_d attaching to the wing surface starts to break; the WTV_d and the TEV_d have detached completely from the wing ($t/T = 0.5$). At the end of the downstroke ($t/T = 0.6$), the detached $LEV_d - WTV_d$, WTV_d , and TEV_d in the wake region form a vortex ring. In Fig. 17, during the upstroke ($t/T = 0.7 - 1$), as the backward wing-flapping speed is larger than the forward flight speed, a leading-edge (LEV_u ; the subscript u denotes forming in the upstroke), trailing-edge (TEV_u), and wing-tip vortices (WTV_u) start to form on the ventral surface of the wing. Similar to those in the downstroke, the LEV_u attaches to the wing surface; the TEV_u detaches from the wing immediately once it forms. Near the wing tip, the annular-shaped WTV_u forms, and a part of the WTV_u merges with the LEV_u , forming a $LEV_u - WTV_u$ structure and detaching from the wing. At the end of the upstroke ($t/T = 1$), the second vortex ring forms, which is constituted by the detached $LEV_u - WTV_u$, WTV_u , and TEV_u generated in the upstroke.

Compared with the cases between $\tau = 0.1$ and $\tau = 0.5$, at about the mid-downstroke ($t/T = 0.2 - 0.4$) and mid-upstroke ($t/T = 0.7 - 0.8$), it is seen that the LEV , WTV , and TEV near the wings in the case with $\tau = 0.1$ are larger than those in the case with $\tau = 0.5$. As a vortex represents a local low-pressure region of fluid, this indicates that the wing surfaces in the case with $\tau = 0.1$ have a larger pressure difference compared with that in the case with $\tau = 0.5$ (as shown in Figs. 16 and 17). In addition, the appearance of the

vortex rings at the end of the downstroke ($t/T = 0.6$) and the upstroke ($t/T = 1$) in the case with $\tau = 0.1$ are clearer and shaped more completely. The vortex rings are considered as a main contribution to generation of lift and thrust in the flight of butterflies [15,16,39]. This suggests that in the case with $\tau = 0.1$, the lift and thrust generated are larger than those in the case with $\tau = 0.5$, as shown in Figs. 15(c) and 15(d).

In Secs. III B and III C, we indicate that the abdominal oscillation with $\tau = 0.1$ causes the thorax-abdomen node to move downward relative to the center of mass in the downstroke and move upward relative to the center of mass in the upstroke. This constructive motion amplifies the flapping speed of the wings relative to the center of mass, and brings the wings to flap against the air drag in an increased speed. The enhanced strength of incoming airflow speed, angle of attack, leading- and trailing-edge vortices, and the pressure difference shown in Figs. 15–17 ($\tau = 0.1$) prove that, via the translational motion between the thorax-abdomen node and the center of mass, the abdominal oscillation with $\tau = 0.1$ increases the lift and thrust generated on the wings. According to our experimental data and preceding reports [9,18–21,23,30], natural butterflies are stated to fly with a particular abdominal phase ($\tau = 0$ or 0.1 in our definition), and do not use other phases. From our analysis, the abdominal phase with $\tau = 0.1$ belongs to the completely constructive case, which maximizes the flapping speed of the wings and generates the greatest lift and thrust (Figs. 12 and 15). It clarifies that natural butterflies utilize this specific range of abdominal oscillating phase to regulate the translational motion between the thorax-abdomen node and the center of mass to enhance flight.

E. Inertial effect caused by thorax, wings, and abdomen

The abdomen oscillating phase recorded from real butterflies ($\tau = 0.1$) generates a constructive motion on the thorax-abdomen node, which speeds up the wing-flapping motion and enhances the aerodynamic force generated on the wings. As this constructive motion of the thorax-abdomen node also contains the inertial effect of head-thorax pitching and wing-flapping motion, in this section we analyze the inertial effect caused by the head-thorax, wings, and abdomen individually.

Figures 18(a) and 18(b) show an inertial force acting on the thorax-abdomen node generated by the head-thorax, wings, and abdomen respectively. The motion of the butterfly model is given based on real butterflies [Eqs. (3)–(5) with $\tau = 0.1$]. In Figs. 18(a) and 18(b), the inertial force generated by the head-thorax is considerably small compared with those generated by the wings and the abdomen. The reason is that the mass of head-thorax is about 30% the total mass of a butterfly (Table I), and the amplitude of head-thorax pitching is about 27° [Fig. 3(b)], less than those of wing-flapping (95°) and abdominal oscillation (55°). On the other hand, the wings possess a much smaller mass ratio (14%; Table I) but have the largest amplitude (95°). The magnitude of inertial force generated by the wings is nearly the same compared with that generated by the abdomen.

For the inertial effect of the head-thorax, wings, and abdomen in different stages of a flapping cycle, according to

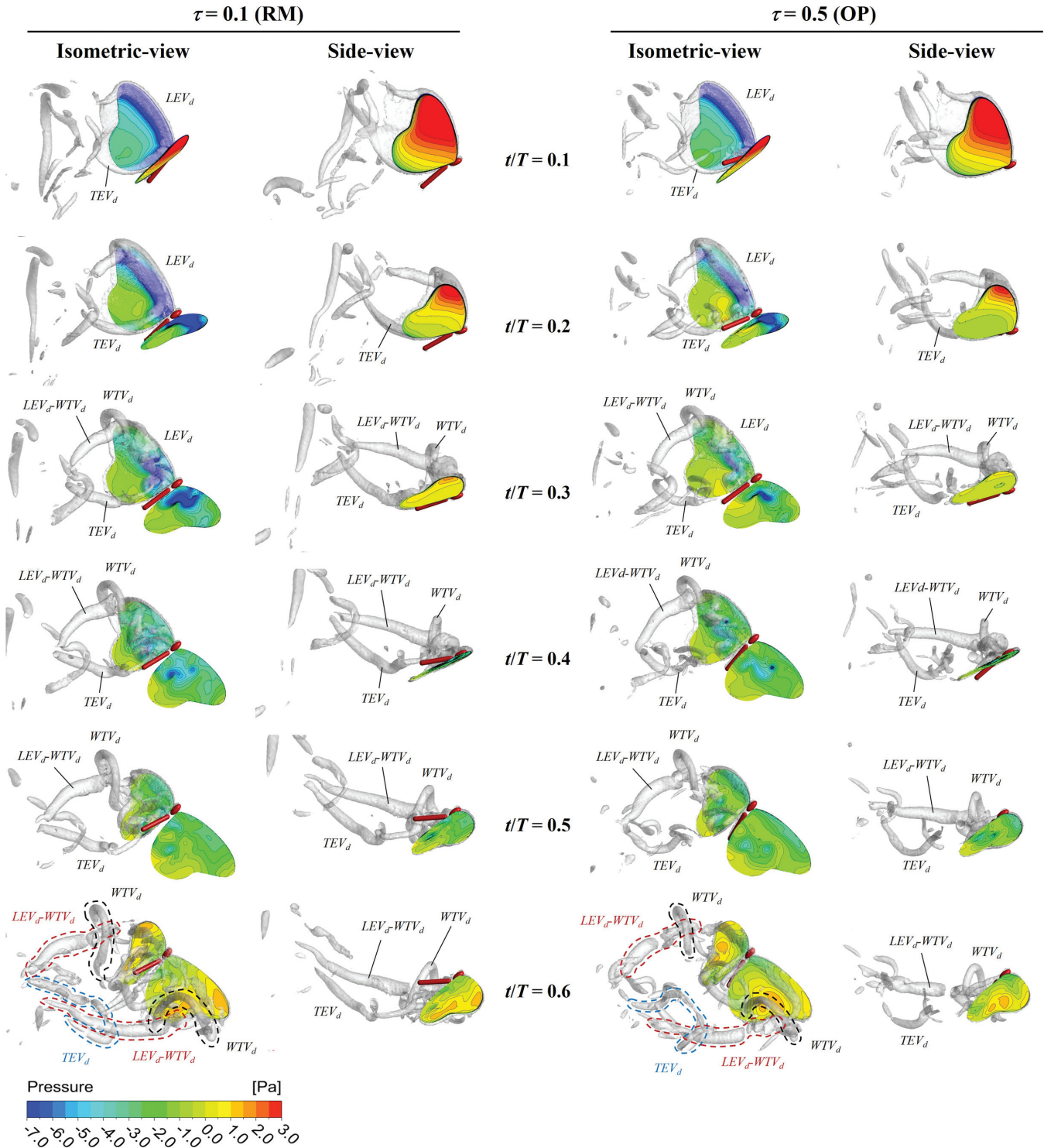


FIG. 16. Pressure contour and vortex structure in cases with (a) the real phase offset of abdominal oscillation ($\tau = 0.1$; RM) and (b) the opposite phase offset of abdominal oscillation ($\tau = 0.5$; OP) during a downstroke. The vortex structure is identified according to the Q criterion with $Q = 33\,090\text{s}^{-2}$, which is 30 times the square of the mean flapping angular velocity.

the kinetics equation [Eq. (17)], we found that there are two individual effects on the motion of the thorax-abdomen node: (i) the wing-flapping motion and abdominal oscillation directly affect the motion of thorax-abdomen node relative to

the center of mass in body frame [the terms in the braces in Eq. (17)], and (ii) the function of head-thorax pitching is to rotate the displacement of thorax-abdomen node relative to the center of mass from the body frame to global

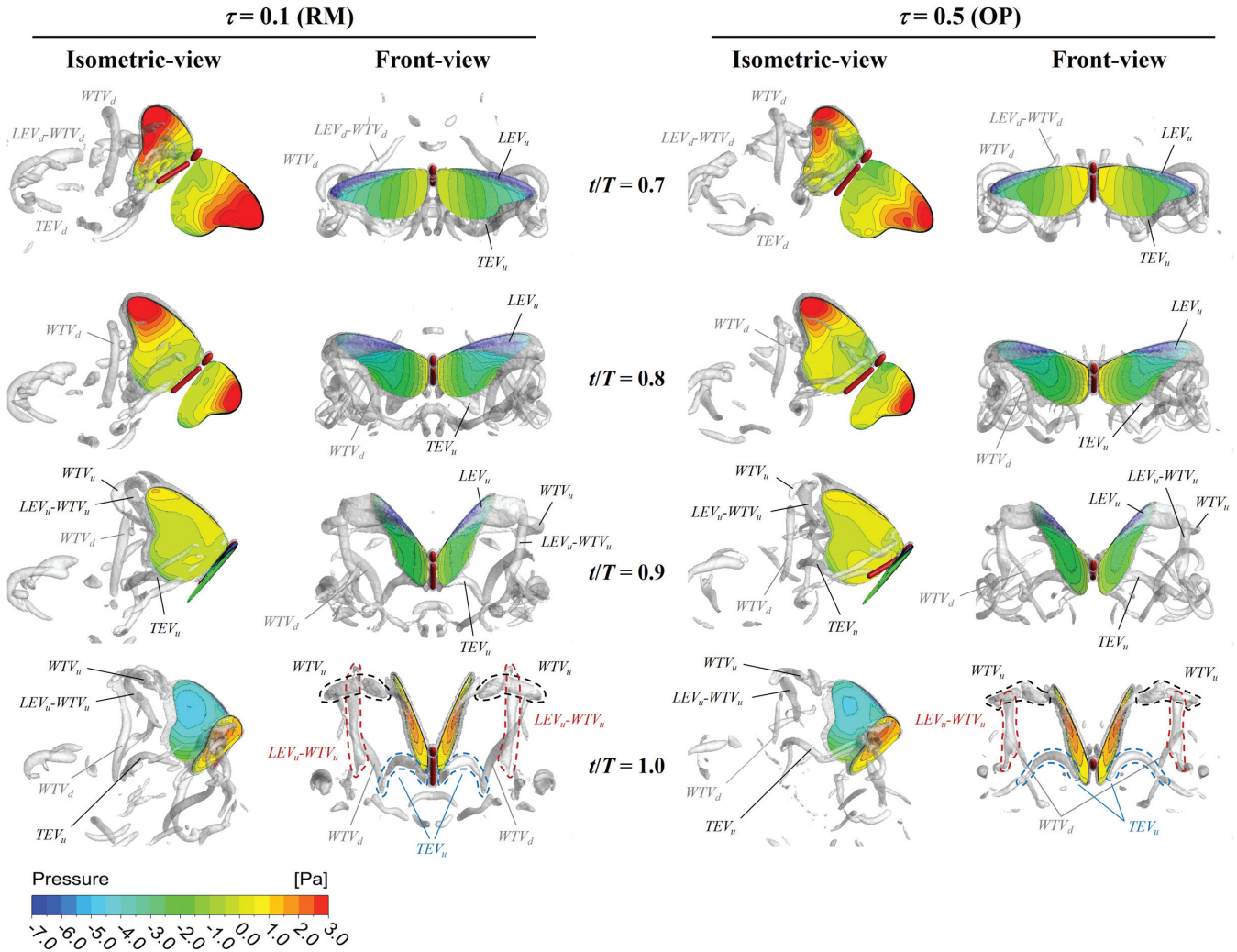


FIG. 17. Pressure contour and vortex structure in cases with (a) the phase offset of abdominal oscillation of a real butterfly ($\tau = 0.1$; RM) and (b) the opposite phase offset of abdominal oscillation ($\tau = 0.5$; OP) during an upstroke. The vortex structure is identified according to the Q -criterion with $Q = 33\,090\text{s}^{-2}$, which is 30 times the square of the mean flapping angular velocity.

frame [the pitching-rotation matrix in left-side in Eq. (17)]. Figure 19 is a schematic diagram. To analyze the motion of the thorax-abdomen node simultaneously caused by the head-thorax pitching, wing-flapping, and abdominal oscillation,

we first separate the displacement contribution of the wing-flapping motion and the abdominal oscillation with analyzing the motion of the thorax-abdomen node in the body frame [Fig. 19(a)], and then analyze the inertial effect of head-thorax

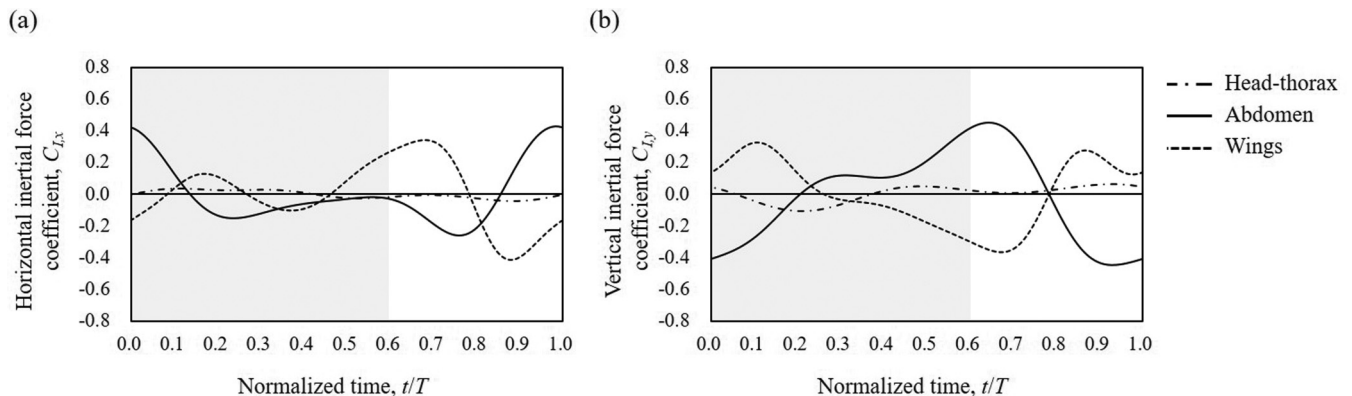


FIG. 18. The inertial force generated by the head-thorax, wings, and abdomen.

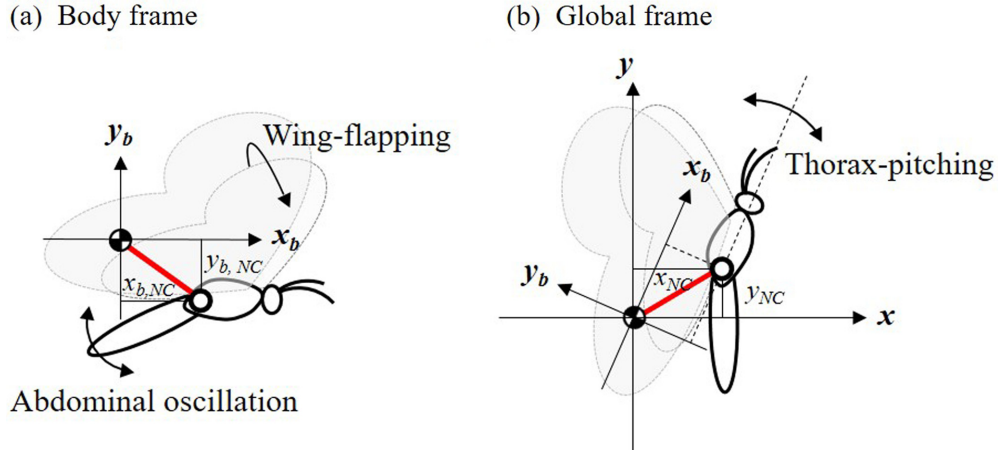


FIG. 19. Effects of head-thorax pitching, wing-flapping, and abdominal oscillation on the translational motion between the thorax-abdomen node and the center of mass. In (a), the translational motion between the thorax-abdomen node and the center of mass in the body frame is affected by the wing-flapping motion and the abdominal oscillation. In (b), the function of head-thorax pitching motion is to rotate the displacement of thorax-abdomen node relative to the center of mass in the global frame.

pitching in the global frame [Fig. 19(b)]:

$$\begin{bmatrix} x_{NC} \\ y_{NC} \\ 0 \end{bmatrix} = - \begin{bmatrix} \cos \theta & -\sin \theta & 0 \\ \sin \theta & \cos \theta & 0 \\ 0 & 0 & 1 \end{bmatrix} \left\{ + \frac{m_T}{m} \begin{bmatrix} r_{AN} \\ 0 \\ 0 \end{bmatrix} + \frac{m_A}{m} \begin{bmatrix} \cos(\psi) & -\sin(\psi) & 0 \\ \sin(\psi) & \cos(\psi) & 0 \\ 0 & 0 & 1 \end{bmatrix} \begin{bmatrix} r_{AN} \\ 0 \\ 0 \end{bmatrix} + \frac{m_{RW}}{m} \begin{bmatrix} 1 & 0 & 0 \\ 0 & \cos \phi & -\sin \phi \\ 0 & \sin \phi & \cos \phi \end{bmatrix} \begin{bmatrix} -r_{RQ} \\ 0 \\ r_{QP} \end{bmatrix} + \frac{m_{LW}}{m} \begin{bmatrix} 1 & 0 & 0 \\ 0 & \cos \phi & \sin \phi \\ 0 & -\sin \phi & \cos \phi \end{bmatrix} \begin{bmatrix} -r_{RQ} \\ 0 \\ -r_{QP} \end{bmatrix} \right\}. \quad (17)$$

Figures 20(a) and 20(b) are respectively the trajectories of the thorax-abdomen node in the body frame and the global frame. The motion of the butterfly model is given based on real butterflies [Eqs. (3)–(5) with $\tau = 0.1$]. In Fig. 20(a), in the early stage of the downstroke ($t/T = 0 - 0.2$), the thorax-

abdomen node moves in the dorsal direction ($+y_b$) relative to the center of mass. This is because in this interval, the wings flap in the ventral direction and the abdomen oscillates down relative to the thorax [Figs. 3(c) and 3(d)]. Nevertheless, in the global frame [Fig. 20(b)], the thorax-abdomen

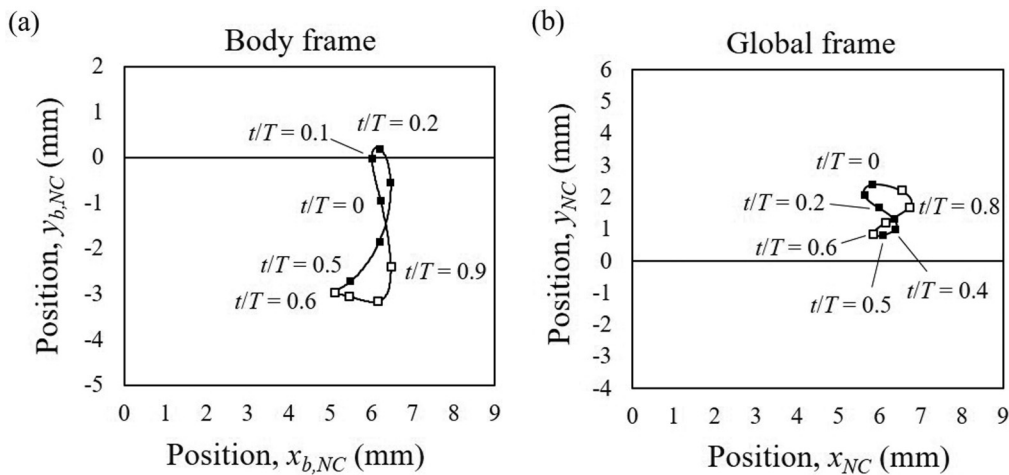


FIG. 20. Trajectories of the thorax-abdomen node relative to the center of mass in (a) body frame and (b) global frame. In each case, the black dot represents the trajectory of the thorax-abdomen node during a downstroke ($t/T = 0 - 0.6$); the white dot represents the trajectory of the thorax-abdomen node during an upstroke ($t/T = 0.6 - 1$). The center of mass of is located at the origin.

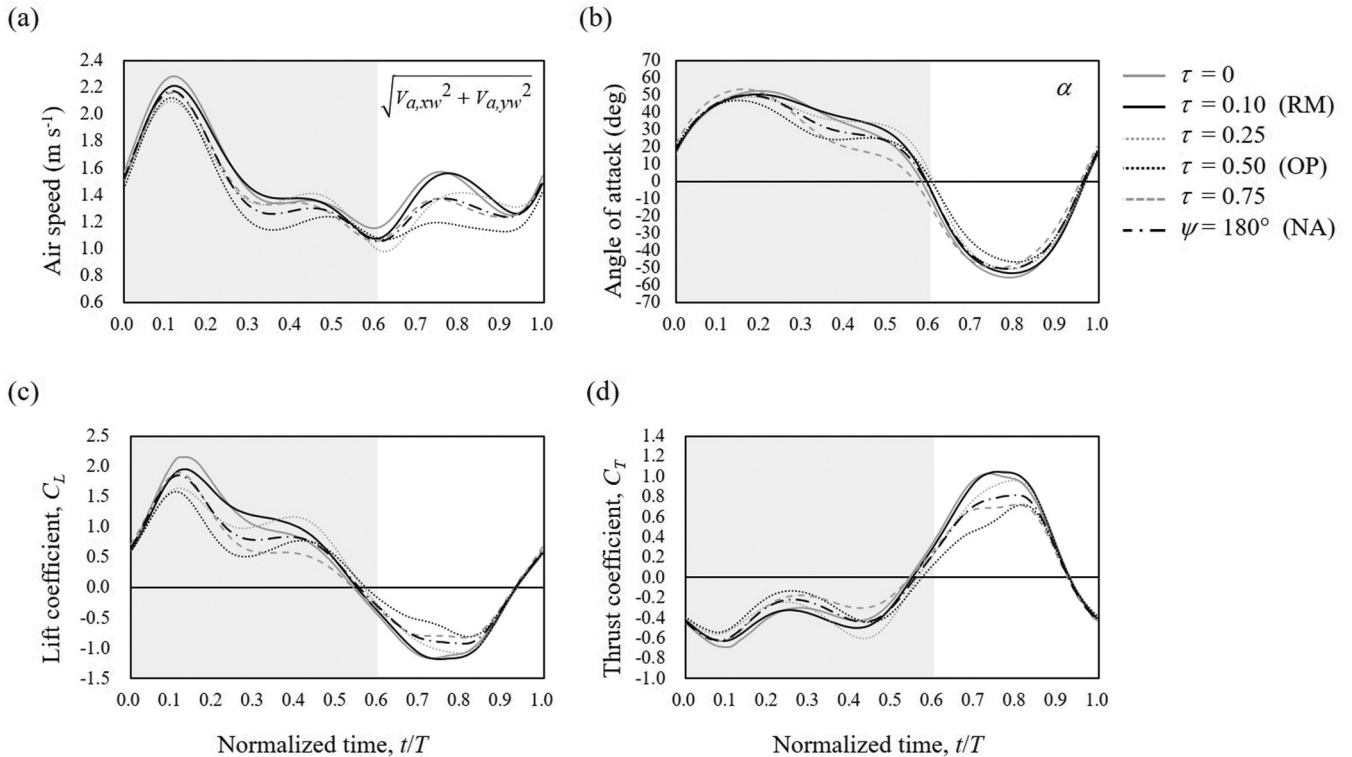


FIG. 21. (a) Speed of incoming airflow, (b) angle of attack, (c) lift coefficient and (d) thrust coefficient on the wings.

node moves downward ($-y$). This indicates that the downward movement of the thorax-abdomen node in the global frame during $t/T = 0 - 0.2$ is mainly due to the pitching-down of the head-thorax. During the rest of the downstroke ($t/T = 0.2 - 0.6$), the thorax-abdomen node begins to move ventrally in the body frame [Fig. 20(a)], and in the global frame it moves downward [Fig. 20(b)]. As during $t/T = 0.2 - 0.6$, the head-thorax pitches up and the wings still flap in the ventral direction [Figs. 3(b)], the ventral movement direction of the thorax-abdomen node in the body frame and the downward movement direction in the global frame are, therefore, due to the oscillating-up movement of the abdomen [Fig. 3(c)]. Last, during the upstroke ($t/T = 0.6 - 1$), the thorax-abdomen node moves dorsally in the body frame [Fig. 20(a)] and upward in the global frame [Fig. 20(b)]. As in this time interval the head-thorax does not pitch obviously and the wings flap dorsally [Figs. 3(b) and 3(d)], the dorsal movement direction of the thorax-abdomen node in the body frame and upward movement direction in the global frame are, therefore, due to the oscillating-down movement of the abdomen [Fig. 3(c)].

To summarize, the inertial force generated by the head-thorax pitching is the smallest, but it strengthens the downward motion of the thorax-abdomen node in the global frame during the early stage of the downstroke ($t/T = 0 - 0.2$). The inertial force generated by the wings has nearly the same magnitude but opposite trend compared with that generated by the abdomen (Fig. 18). From the analysis of motions in both body frame and global frame, it is concluded that the abdominal oscillation is the main factor that makes the thorax-abdomen node move downward relative to the

center of mass in the downstroke and move upward relative to the center of mass in the upstroke in the global frame. This constructive motion of the thorax-abdomen node thus speeds up the wing-flapping speed relative to the center of mass, and further enhances the lift and thrust generated on the wings.

IV. CONCLUSION

We conducted experiments and numerical simulations to investigate the effect of abdominal oscillation on the translational motion between the thorax-abdomen node and the center of mass, and the resulting aerodynamic force in a free-flying butterfly (*Idea leuconoe*). The numerical model was verified on comparison with the data for flight velocity measured in the experiment.

Butterflies fly with an abdomen oscillating relative to thorax; the abdominal oscillation causes the thorax-abdomen node to move translationally relative to the center of mass of a butterfly. With fixed motional functions of the head-thorax pitching and the wing-flapping, the numerical results show that the abdominal oscillation significantly changes the motion of the thorax-abdomen node relative to the center of mass. The instantaneous values of lift and thrust generated on wings are increased by 50.32% and 32.57% respectively compared to the case of no abdominal oscillation. With the abdominal oscillation recorded from the experiment, the abdomen causes the thorax-abdomen node to move downward relative to the center of mass in the downstroke and upward relative to the center of mass in the upstroke. This constructive motion

amplifies the flapping speed of wings relative to the center of mass. The movement direction of the thorax-abdomen node relative to the center of mass is also opposite to air drag. The wings, thereby, obtain an increased flapping speed to flap against the air drag, and improve the lift and the thrust. Flow analysis shows that the abdominal oscillation increases the angle of attack and the speed of airflow striking the wings; the strength of leading- and trailing-edge vortices on the wings is enhanced. On comparison of the inertial forces generated by the head-thorax, wings, and abdomen, the results show that the inertial force generated by the abdominal oscillation is the main factor to constitute the constructive motion of the thorax-abdomen node. According to our experimental data and preceding reports, natural butterflies are stated to utilize a particular phase offset of abdominal oscillation to fly, and do not use other phases. From our analysis, this phase offset leads the thorax-abdomen node to move relative to the center of mass in the same direction of the wing-flapping during a whole cycle, which produces a completely constructive motion on the thorax-abdomen node and maximizes the lift and thrust on the wings. It clarifies that real butterflies utilize this specific range of abdominal oscillating phase to regulate the translational motion between the thorax-abdomen node and the center of mass to enhance flight.

Previous authors have shown that the abdominal oscillation produces an inertial torque to alter the thorax-pitching of a

butterfly. The translational mechanism presented in this paper, that the abdominal oscillation produces an inertial force to control the translational motion between the thorax-abdomen node and the center of mass, shows an equally important role as the effect of thorax-pitching. This work might provide insight into flight of butterflies and for the design of micro aerial vehicles.

ACKNOWLEDGMENTS

National Taiwan University partially supported this work under Contract No. NTU-CC-109L893301. The Taiwan Ministry of Science and Technology also partially supported this work under Contract No. MOST 108-2221-E-002-046. We thank Dr. Ogilvie for suggestions and discussion.

APPENDIX

Figure 21 shows the speed of incoming airflow, angle of attack, lift coefficient and thrust coefficient acting on the wings among varied abdominal oscillation phases (τ). Overall, the oscillating phases recorded from the real butterfly ($\tau = 0$ and 0.1) have the largest speed of incoming airflow and the angle of attack, resulting the largest magnitude of the lift and the thrust. In contrast, the opposite oscillating phase ($\tau = 0.5$) has the smallest incoming airflow and the angle of attack, resulting the smallest magnitude of the lift and the thrust.

-
- [1] W. Shyy, H. Aono, C. K. Kang, and H. Liu, *An Introduction to Flapping Wing Aerodynamics* (Cambridge University Press, New York, 2013).
 - [2] R. Dudley and R. B. Srygley, *J. Exp. Biol.* **191**, 125 (1994).
 - [3] H. Tanaka and I. Shimoyama, *Bioinspir. Biomim.* **5**, 026003 (2010).
 - [4] C. P. Ellington, C. van den Berg, A. P. Willmott, and A. L. R. Thomas, *Nature (London)* **384**, 626 (1996).
 - [5] J. M. Birch and M. H. Dickinson, *Nature (London)* **412**, 729 (2001).
 - [6] D. Lentink and M. H. Dickinson, *J. Exp. Biol.* **212**, 2705 (2009).
 - [7] Y. Lee, K. Lua, and T. Lim, *Bioinspir. Biomim.* **11**, 056013 (2016).
 - [8] H. Takahashi, H. Tanaka, K. Matsumoto, and I. Shimoyama, *Bioinspir. Biomim.* **7**, 036020 (2012).
 - [9] M. Sridhar, C. K. Kang, and D. B. Landrum, *46th AIAA Fluid Dynamics Conference* (Washington, DC, 2016).
 - [10] A. P. Willmott and C. P. Ellington, *J. Exp. Biol.* **200**, 2723 (1997).
 - [11] P. Y. Zou, Y. H. Lai, and J. T. Yang, *Phys. Rev. E* **100**, 063102 (2019).
 - [12] A. L. R. Thomas, G. K. Taylor, R. B. Srygley, R. L. Nudds, and R. J. Bomphrey, *J. Exp. Biol.* **207**, 4299 (2004).
 - [13] R. Dudley, *J. Exp. Biol.* **150**, 37 (1990).
 - [14] C. K. Kang, J. Cranford, M. K. Sridhar, D. Kodali, D. B. Landrum, and N. Slegers, *AIAA J.* **56**, 15 (2018).
 - [15] Y. H. J. Fei and J. T. Yang, *Phys. Rev. E* **93**, 033124 (2016).
 - [16] H. Huang and M. Sun, *Acta. Mech. Sin.* **28**, 1590 (2012).
 - [17] T. Lin, L. Zheng, T. Hedrick, and R. Mittal, *Bioinspir. Biomim.* **7**, 044002 (2012).
 - [18] K. Senda, T. Obara, M. Kitamura, N. Yokoyama, N. Hirai, and M. Iima, *Bioinspir. Biomim.* **7**, 025002 (2012).
 - [19] K. Senda, T. Obara, M. Kitamura, T. Nishikata, N. Hirai, M. Iima, and N. Yokoyama, *Robot Auton. Syst.* **60**, 670 (2012).
 - [20] T. Fujikawa, K. Hirakawa, S. Okuma, T. Udagawa, S. Nakano, and K. Kikuchi, *Mech. Syst. Signal Process* **22**, 1304 (2008).
 - [21] S. Sunada, K. Kawachi, I. Watanabe, and A. Azuma, *J. Exp. Biol.* **183**, 249 (1993).
 - [22] T. Wilson and R. Albertani, *52nd AIAA Aerospace Science Meeting* (National Harbor, MD, 2014).
 - [23] N. Yokoyama, K. Senda, M. Iima, and N. Hirai, *Phys. Fluids* **25**, 021902 (2013).
 - [24] K. Suzuki, K. Minami, and T. Inamuro, *J. Fluid Mech.* **767**, 659 (2015).
 - [25] J. Jayakumar, K. Senda, and N. Yokoyama, *J. Aircr.* **55**, 2327 (2018).
 - [26] K. Suzuki, T. Aoki, and M. Yoshino, *Fluid Dyn. Res.* **49**, 055504 (2017).
 - [27] K. Suzuki, I. Okada, and M. Yoshino, *J. Fluid Mech.* **877**, 614 (2019).
 - [28] C. K. Kang, M. Sridhar, and D. B. Landrum, *2018 AIAA Aerospace Sciences Meeting* (Kissimmee, FL, 2018).
 - [29] M. Sridhar, C. K. Kang, and D. B. Landrum, *AIAA SciTech 2019 Forum* (San Diego, CA 2019).
 - [30] M. Sridhar, C. K. Kang, and T. Lee, *AIAA SciTech 2020 Forum* (Orlando, FL, 2020).
 - [31] Y. H. J. Fei and J. T. Yang, *Phys. Rev. E* **92**, 033004 (2015).
 - [32] J. Y. Su, S. C. Ting, Y. H. Chang, and J. T. Yang, *Phys. Rev. E* **84**, 012901 (2011).

- [33] J. Y. Su, S. C. Ting, Y. H. Chang, and J. T. Yang, *J. R. Soc. Interface* **9**, 1674 (2012).
- [34] Y. H. Lai, Y. J. Lin, S. K. Chang, and J. T. Yang, *Bioinspir. Biomim.* (2020), doi:[10.1088/1748-3190/abc293](https://doi.org/10.1088/1748-3190/abc293).
- [35] K. B. Lua, T. T. Lim, and K. S. Yeo, *AIAA J.* **52**, 1095 (2014).
- [36] R. B. Srygley and A. L. R. Thomas, *Nature (London)* **420**, 660 (2002).
- [37] S. P. Sane, *J. Exp. Biol.* **206**, 4191 (2003).
- [38] A. Banerjee, S. K. Ghosh, and D. Das, *ISRN Mech. Eng.* **2011**, 162687 (2011).
- [39] M. Fuchiwaki, T. Kuroki, K. Tanaka, and T. Tababa, *Exp. Fluids* **54**, 1450 (2013).
- [40] S. K. Jones, R. Laurenza, T. L. Hedrick, B. E. Griffith, and L. A. Miller, *J. Theor. Biol.* **384**, 105 (2015).